ISSN 0869-5911, Petrology, 2006, Vol. 14, No. 2, pp. 154–186. © Pleiades Publishing, Inc., 2006.
Original Russian Text © G.V. Ledneva, A.A. Nosova, A.V. Soloviev, 2006, published in Petrologiya, 2006, Vol. 14, No. 2, pp. 168–202.

"Calc–Alkaline" Magmatism of the Omgon Range: Evidence for Early Paleogene Extension in the Western Kamchatka Segment of the Eurasian Continental Margin

G. V. Ledneva *, A. A. Nosova **, and A. V. Soloviev *

** Geological Institute (GIN), Russian Academy of Sciences, Pyzhevskii per. 7, Moscow, 109017 Russia*

e-mail: ledneva@ilran.ru, Solov@ilran.ru

*** Institute of the Geology of Ore Deposits, Petrography, Mineralogy, and Geochemistry (IGEM), Russian Academy of Sciences, Staromonetnyi per. 35, Moscow, 109017 Russia*

e-mail: nosova@igem.ru

Received December 18, 2004

Abstract—The hypabyssal rocks of the Omgon Range, western Kamchatka, that intrude Upper Albian–Lower Campanian deposits of the Eurasian continental margin belong to three coeval (62.5–63.0 Ma) associations: (1) ilmenite gabbro-dolerites, (2) titanomagnetite gabbro-dolerites and quartz microdiorites, and (3) porphyritic biotite granites and granite-aplites. The Early Paleocene age of the ilmenite gabbro-dolerites and biotite granites was confirmed by zircon and apatite fission-track dating. The ilmenite and titanomagnetite gabbro-dolerites were produced by the multilevel fractional crystallization of basaltic melts with, respectively, moderate and high Fe–Ti contents and the contamination of these melts with rhyolitic melts of different compositions. The moderate- and high-Fe–Ti basaltic melts were derived from mantle spinel peridotite variably depleted and metasomatized by slab-derived fluid prior to melting. The melts were generated at variable depths and different degrees of melting. The biotite granites and granite aplites were produced by the combined fractional crystallization of a crustal rhyolitic melt and its contamination with terrigenous rocks of the Omgon Group. The rhyolitic melts were likely derived from metabasaltic rocks of suprasubduction nature. The Early Paleocene hypabyssal rocks of the Omgon Range were demonstrated to have been formed in an extensional environment, which dominated in the margin of the Eurasian continent from the Late Cretaceous throughout the Early Paleocene. Extension in the Western Kamchatka segment preceded the origin of the Western Koryakian–Kamchatka (Kinkil') continental-margin volcanic belt in Eocene time. This research was conducted based on original geological, mineralogical, geochemical, and isotopic (Rb–Sr) data obtained by the authors for the rocks.

DOI: 10.1134/S0869591106020020

INTRODUCTION

Within the scope of the plate tectonics model, indicator compositional parameters of volcanic rocks are widely used, together with structural and other geologic information, to interpret the geodynamic environments in which rocks composing foldbelts were formed (Miyashiro, 1974; DePaolo and Wasserburg, 1976; Wood, 1980; Pearce *et al.*, 1984; Cabanis and Lecolle, 1989; LeMaitre *et al.*, 1989; Gorton and Schandl, 2000; Condie, 2001). However, igneous rocks often display dualistic petrotectonic signatures, and this precludes the direct utilization of the petrochemical, geochemi-

Fig. 1. Schematic map of the distribution of Lower Cretaceous–Cenozoic continental-margin volcanic belts and magmatic areas related to extension zones in the Kamchatka and Penzhina–Anadyr–Koryakia regions (modified after *Tectonic Map…*, 1992, 2000; Fedorov and Filatova, 1999). The outlined area was examined in detail by Fedorov and Filatova (1999).

Continental-margin volcanic belts: (*1*) Okhotsk–Chukchi (Albian–Campanian), (*2*) Western Kamchatka–Koryakia (Middle Eocene–Oligocene), (*3*) Sredinnyi range of Kamchatka (*a*—Miocene–Pliocene, *b*—Pliocene–Quaternary), (*4*) Kurile–Kamchatka island arc (Pliocene–Quaternary). Magmatic complexes of extension zones: (*5*) Maestrichtian–Middle Eocene (*a*—volcanic areas, *b*—dike swarms, sills, and small intrusions), (*6*) Neogene–Quaternary. Boundaries: (*7*) stratigraphic, (*8*) normal faults; (*9*) strike-slip faults, (*10*) faults of uncertain kinematics (*a*—documented, *b*—inferred).

Circled numerals indicate areas of Maestrichtian–Middle Eocene volcanic and hypabyssal rocks of extension zones, which are described in (Slyadnev *et al.*, 1997; Shantser and Fedorov, 1997; Fedorov and Filatova, 1999; Palandzhyan, 2002; this publication). Areas of hypabyssal rocks: (*1*) Omgon Range, (*2*) Elistratov Peninsula, (*3*) Talovka Mountains (Kuyul Massif), (*4*) El'denyr Massif, (*5*) Ust'-Belaya Massif, (*6*) Pekul'ney Range, (*7*) Rarytkin Range. Areas of volcanic rocks: (*8*) western slopes of the Sredinnyi Range of Kamchatka (Cherepanov Series), (*9*) Utkholok Peninsula, (*10*) Evdyrveem, (*11*) Chineyveem, (*12*) Kanchalan–Tanyurer, (*13*) Rarytkin, (*14*) Anadyr depression, (*15*) Kakanaut, (*16*) Vel'kemveem. Dashed lines mark fields of rocks of similar composition in western Kamchatka and Koryakia.

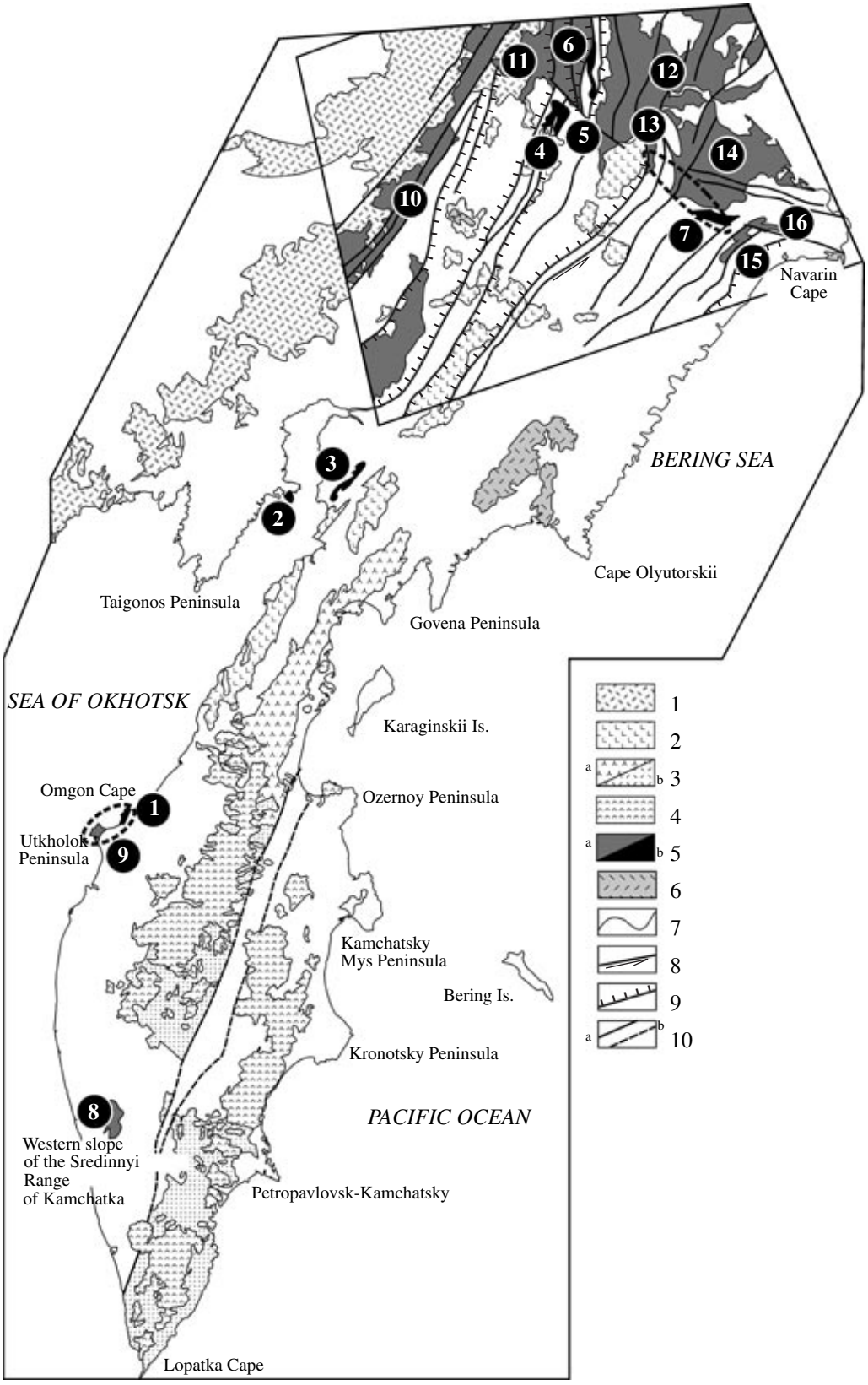
6
11
12
13
5
4
14
10
7
16
15
Navarin Cape
BERING SEA
3
2
Cape Olyutorskii
Taigonos Peninsula
Govena Peninsula
SEA OF OKHOTSK
Karaginskii Is.
Omgon Cape
1
Ozernoy Peninsula
Utkholok Peninsula
9
Kamchatsky Mys Peninsula
Bering Is.
Kronotsky Peninsula
PACIFIC OCEAN
8
Western slope of the Sredinnyi Range of Kamchatka
Petropavlovsk-Kamchatsky
Lopatka Cape
1
2
a b 3
4
a b 5
6
7
8
9
a b 10

cal, and isotopic geochemical data. Rocks with "mixed" petrotectonic signatures can likely be produced in diverse geodynamic environments. Striking examples are offered by (i) volcanic rocks of intra- and backarc basins, (ii) magmatic rocks in extensional areas and continental-margin rifts, such as the Basin and Range Province in the western North American coast (Robyn, 1979; Goles, 1986; Falkner *et al.*, 1995; Hawkesworth *et al.*, 1995; Hooper *et al.*, 1995, 2002; Johnson and Grunder, 2000; Morris *et al.*, 2000; Camp *et al.*, 2003), the coastal areas of central Queensland, West Australia (Ewart *et al.*, 1992), the D'Entrecasteaux Islands, eastern Papua New Guinea (Smith, 1976; Smith and Milsom, 1984); and (iii) continental-margin volcanic rocks generated above a slab window, as near the Taitao Peninsula, where the West Chile Rise is subducted beneath the South American plate (Guivel *et al.*, 1999; D'Orazio *et al.*, 2003).

Volcanic and intrusive rocks with mixed petrotectonic signatures can be produced by various processes, such as (i) the adiabatic melting of a lithospheric mantle source that has undergone metasomatic recycling by fluids and/or melts from the subducted plate, as is typical of extensional environments and rifting in continental margins; (ii) interaction between lithospheric and asthenospheric mantle sources, which is process possible when a mid-oceanic ridge is subducted and induces the development of a window in the subducted slab; and (iii) the modification of parental melts within the crust due to assimilation (contamination), mixing, and other processes. Different geodynamic environments are characterized by different processes that can generate melts and maintain their further evolution. This predetermines the importance of petrologic research focused on the simulation of the compositions of parental melts and the contribution of various sources and magma-transforming mechanisms within the crust when geodynamic interpretations are accomplished based on data on the composition of igneous rocks.

This publication presents an illustration of the dependence of a geodynamic interpretation on the model proposed for the genesis of magmatic rocks with reference to Lower Paleocene hypabyssal rocks in the coastal cliffs of the Omgon Range in western Kamchatka (Figs. 1, 2a–2c). The dualistic petrotectonic affiliation of these magmatic complexes, which were produced *in situ*, and the scarcity of information on their composition were largely responsible for the contradictoriness of the concepts proposed to account for the tectonic development of the Western Kamchatka segment of the Eurasian continental margin at the boundary between the Late Maestrichtian and Early Paleocene. According to some geologists (Seliverstov, 1998; Bogdanov, 2000), this area was then an Eurasian continental margin; while others researchers (Konstantinovskaya, 2003) believe that it was a intracontinental area. The type of this margin is also poorly understood as of yet. In geological reconstructions, this lithospheric plate boundary can be shown as convergent (subduction-related; Seliverstov, 1998), collisional (Bogdanov, 2000), or transform (Bogdanov, 2000).

Until recently, precise analytical data on the composition of the Lower Paleocene rocks from western Kamchatka were limited only to four samples of basalt, andesite, dacite, and rhyolite from the Utkholok Peninsula. According to Shantser and Fedorov (1997), these rocks have a composition analogous to that of continental-margin volcanics of the calc–alkaline series that crystallized from melts derived during the partial melting of "rocks in the mantle wedge zone above the seismic focal plane." This interpretation has underlain the conclusion that the Lower Paleocene volcanics of western Kamchatka should be classed with the rocks of the Western Koryakia–Kamchatka (Kinkil') marginal volcanic belt.

This conclusion is, however, in conflict with modern interpretations of the geodynamic evolution of adjacent areas of the Pacific at the boundary between the Late Maestrichtian and Early Paleocene, a fact that triggered the development of alternative hypotheses proposed to account for the geodynamic evolution of the area (Seliverstov, 1998; Bogdanov, 2000; Konstantinovskaya, 1999, 2001). The geodynamic evolutionary models are somewhat different. However, there is convincing evidence that the Northwest Pacific hosted at that time a system of island arcs and related fore-, intra-, and backarc basins, whose fragments are now preserved in the form of exotic terranes in western Kamchatka (Kuz'michev and Sukhov, 2000; Kovalenko *et al.*, 2005), Govena–Karaginskii zone (Chek-

Fig. 2. Geological map of the Omgon Range.

(a) Location of the study area.

(b) Geologic structure of the Omgon Range [prepared by A.V. Lander, A.V. Soloviev, G.V. Ledneva, and V.E. Verzhbitskii with the use of materials from (Singaevskii and Babushkin, 1965; *Geological Map...,* 1989; Bondarenko and Sokolkov, 1990; Bogdanov *et al.*, 1991).

(*1*) Quaternary deposits; (*2*) Snatol Series, terrigenous deposits (Middle Eocene); (*3*) Snatol Series, conglomerates (Middle Eocene); (*4*) Omgon Group, turbidites (Albian–Campanian); (*5*) Omgon Group, conglomerates (Cretaceus); (*6*) complex of siliceous and volcanic rocks: pillow basalts, dolerite-basalts and dolerites, cherts, limestones (Middle Jurassic–Lower Cretaceous); (*7*) cherts (Upper Jurassic); (*8*) sills of subvolcanic rocks: (*a*) of predominantly acid–ultracid composition, (*b*) basic–intermediate composition (Early Paleocene); (*9*) faults: (*a*) overthrusts, (*b*) subvertical, (*c*) inferred; (*10*) contacts: (*a*) unconformable, (*b*) stratigraphic; (*11*) strike and dip symbols.

(c) Sampling sites.

(d) Principal structural scheme of thick sills that consist mostly of mafic–intermediate rocks (not to scale).

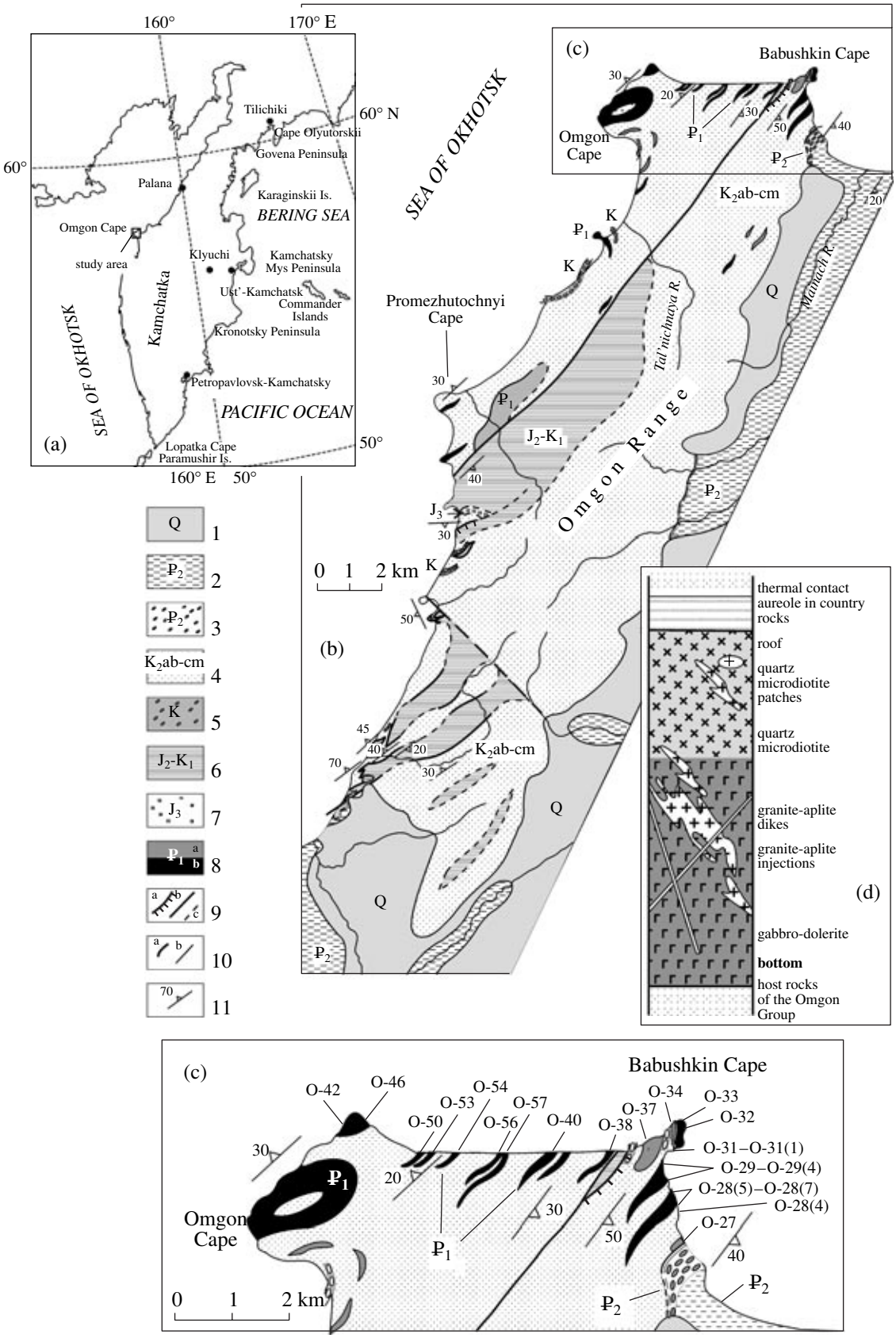
160°
170° E
60° N
60°
50°
160° E
50°
Tilichiki
Cape Olyutorskii
Govena Peninsula
Palana
Karaginskii Is.
BERING SEA
Omgon Cape
study area
Klyuchi
Kamchatsky Mys Peninsula
Ust'-Kamchatsk
Commander Islands
Kronotsky Peninsula
Kamchatka
SEA OF OKHOTSK
Petropavlovsk-Kamchatsky
PACIFIC OCEAN
Lopatka Cape
Paramushir Is.
(a)
SEA OF OKHOTSK
(c)
Babushkin Cape
Omgon Cape
Promezhutochnyi Cape
Tal'nichnaya R.
Mamach K.
Omgon Range
(b)
0 1 2 km
Q 1
P2 2
P2 3
K2ab-cm 4
K 5
J2-K1 6
J3 7
P1 a b 8
9
10
70 11
thermal contact aureole in country rocks
roof
quartz microdiotite patches
quartz microdiotite
granite-aplite dikes
granite-aplite injections
gabbro-dolerite
bottom
host rocks of the Omgon Group
(d)
O-42
O-46
O-54
O-53
O-57
O-50
O-56
O-40
O-38
O-34
O-33
O-37
O-32
O-31–O-31(1)
O-29–O-29(4)
O-28(5)–O-28(7)
O-28(4)
O-27

hovich *et al.*, 1990), and East Ranges and East Peninsulas of Kamchatka (Zinkevich *et al.*, 1993). These data testify that the ocean-continent transition zone belonged to the West Pacific type, which is characterized by passive continental margins (Khain and Lomize, 1995).

This publication presents the very first data on the composition of Lower Paleocene rocks of the Omgon Range. Analysis of these data together with literature materials on volcanics from western Kamchatka and adjacent areas allowed us to give a justified and realistic geodynamic interpretation, which is consistent with geological, paleomagnetic, and other data. This study was based on our original materials on the geology, mineralogy, major- and trace-element chemistry, and isotopic geochemistry of local rocks, on the calculated thermodynamic conditions under which these rocks were formed, and on the simulation of the magmatic processes.

GENERAL GEOLOGICAL OVERVIEW AND THE SETTING OF HYPABYSSAL ROCKS IN THE OMGON RANGE

Geological overview. Interpretations of the structure of the western Kamchatka basement are contradictory. Some researchers believe that western Kamchatka is a continental or subcontinental block that collided with Eurasia (Parfenov and Natal'in, 1997; Khanchuk, 1985; Zonenshain *et al.*, 1990; Gladenkov *et al.*, 1997; Konstantinovskaya, 2001, 2003). Others distinguish an individual western Kamchatka continental microplate (Bogdanov, 2000; Bogdanov and Chekhovich, 2002), which existed in Cretaceous time and collided with the Sea of Okhotsk plate in the Maestrichtian. Soloviev (2005) argues that western Kamchatka is an accretionary-collision belt that consists of three structural units, with an autochthon (or a parautochthon), allochthon, and a neoautochthon.

The **autochthon** (or parautochthon) is made up of terrigenous (mudstone, siltstone, and sandstone), in places flyschoid sequences (Soloviev, 2005), which were likely deposited on a margin of the Eurasian continent. According to the fission-track datings of the detrital zircon (Soloviev, 2005) and fossil ages (ammonites, aptychi, bivalves, and gastropods; Palechek *et al.*, 2005), the timing of the sedimentation varies from place to place, with the overall time span constrained to the Aptian–Albian. Sandstones are compositionally similar throughout the area and correspond to quartz–feldspar and feldspar–quartz graywacke. The terrigenous complex was deposited on a continental margin. The mineralogy of the sandstones (Goldyrev, 2001; Shapiro *et al.*, 2001) and the chemistry of the mudstones (Bogdanov *et al.*, 2003; Soloviev *et al.*, 2005) suggest that the material was transported from a dissected volcanic arc (most probably, the Okhotsk–Chukchi volcanic belt), which started to develop on the basement of the Eurasian paleomargin (Soloviev, 2005; Soloviev *et al.*, 2005).

The autochthonous continental-margin sequences of the Omgon Range bear tectonic blocks and nappes consisting of Middle Jurassic–Early Cretaceous (Bondarenko and Sokolkov, 1990; Vishnevskaya *et al.*, 1998; Bogdanov *et al.*, 2003; Soloviev *et al.*, 2005) pillow dolerite-basalts and basalts of the N-MORB type and their derivatives (basaltic andesites), which were erupted at the seafloor, with cherty and jasper material filling the space between pillows and occurring as individual blocks (Bogdanov *et al.*, 2003; Soloviev *et al.*, 2005). Blocks of Late Jurassic–Early Cretaceous age are contained in the accretionary prism of the Okhotsk–Chukchi continental-margin volcanic belt. The accretionary prism was formed during the subduction of oceanic plates (Izanagi and Kula) beneath the Eurasian continental margin. The development of the prism ended in the Maestrichtian (~70 Ma; Bogdanov *et al.*, 2003; Soloviev *et al.*, 2005).

The **allochthon** is composed of Upper Cretaceous complexes, which consist of spatially separated tectonic nappes occurring as an extended (~500 km) longitudinal belt. Individual nappes consist of Coniacian–Lower Campanian volcanic–siliceous deposits (Vishnevskaya *et al.*, 2005), Campanian–Maestrichtian volcanic–terrigenous deposits (Kurilov, 2000) with Maestrichtian dolerite and Early Paleocene dolerite and granite-aplite sills (Sukhov and Kuz'michev, 2005) and volcanic rocks erupted at the boundary between the Campanian and Maestrichtian (Palechek *et al.*, 2003). The source of material for the volcanic–terrigenous sequences was a volcanic arc (Ledneva, 2002; Sukhov and Kuz'michev, 2005). According to paleomagnetic data, the Campanian–Maestrichtian volcanic–terrigenous sequences were accumulated at ~40° N, at a significant distance form the ancient Eurasian continental margin (Kovalenko, 2003).

The allochthonous rocks are considered to compose the separate Omgon–Palana collision belt (Bogdanov, 2000; Bogdanov and Chekhovich, 2002) or to be the fragments of a sometime-continuous island arc (referred to as the Kvakhona arc; Konstantinovskaya, 2003), which were obducted over the continental basement. Some researchers include these Upper Mesozoic deposits in the Achaivayam–Valaginsky arc, which combines fragments of Upper Cretaceous sequences from the Koryak Highland, western Kamchatka, the southern portion of the Sredinnyi Range, and the East Ranges of Kamchatka (Shapiro, 1995).

The Upper Cretaceous allochthonous rocks are overlain by molasses of the *neoautochthon*, whose age is still not constrained reliably enough. The deposits of the Anadyrka Series overlain (with a sharp discontinuity; Palechek *et al.*, 2003) the deformed Cretaceous tuff–sedimentary rocks of the Palana sequence. The conglomerates and sandstones of the Anadyrka Formation (which is also referred to as the Khulgun Forma-

tion) are of Paleocene age (Gladenkov *et al.*, 1997). These authors point out that "the stratigraphic position of the Anadyrka Formation should be regarded as provisional until newly obtained data make it possible to constrain it more accurately." However, according to A.E. Shantser (personal communication), recent biostratigraphic materials point to an Eocene age of the Anadyrka Formation. Now its dating cannot be regarded as unambiguous. The neoautochthonous deposits of the Snatol Formation, which are widespread in western Kamchatka, seem to be dated reliably enough at the Middle Eocene (Gladenkov *et al.*, 1997).

Setting of the Omgon Range hypabyssal rocks. Lower Paleocene hypabyssal rocks occur in the Omgon Range as numerous sills that intrude the autochthonous deposits (Figs. 2b, 2d): siltstone, mudstone, and sandstone (corresponding to quartz–feldspar graywacke of the Upper Albian–Lower Campanian continental-margin terrigenous complex, which is combined into the Omgon Group; Soloviev *et al.*, 2005). According to paleomagnetic data, the spatial position of the Omgon rocks during the emplacement of the sills was close to their modern position (Chernov and Kovalenko, 2001; Kovalenko, 2003). Thus, the Omgon Range hypabyssal rocks mark the postaccretionary evolution of the continental margin in the Early Paleocene.

INNER STRUCTURE OF THE SILLS AND THEIR RELATIONS WITH THE HOST ROCKS OF THE OMGON GROUP

The sills consist of ilmenite and titanomagnetite gabbro-dolerites, quartz microdiorites, porphyritic biotite granites, and granite-aplites. The mafic–intermediate and acid–hyperacid hypabyssal rocks compose either individual sills or occur within a single body and are then characterized by intrusive relations.

The relatively thin (approximately 1–5 m) sills have simple inner structures and commonly consist only of one of the aforementioned rock types. The inner-contact zones of the sills are made up of micro- and fine-grained rocks that grade into coarser grained varieties toward the central parts of the bodies. Thick (about 30–200 m) sills of mafic–intermediate composition have a "differentiated" inner structure: the bulk of the bodies is composed of gabbro-dolerites and quartz microdiorites, which grade into one another in the vertical section (Fig. 2d). Granophyric varieties are rare and occur as small elongated lenses (from 1–2 to 10–15 cm along the long axes of the ellipses) among patchy quartz microdiorites. Where contained in mafic and intermediate sills, granite-aplites compose either thin (5–10 cm) randomly oriented veins or injections whose thicknesses and strikes vary and which are oriented roughly parallel to the contact zones.

Thick (up to 30–40 m) granite-aplite sills contain xenoliths of the host terrigenous rocks of the Omgon Group and are sometimes cut by relatively thin (10–15 cm) veins of titanomagnetite gabbro-dolerites. The geologic relations between the hypabyssal rocks of mafic–intermediate and acid–hyperacid composition suggest that all of them were emplaced simultaneously; the granitoids were intruded in several stages.

The mafic–intermediate sills are surrounded by outer-contact thermal aureoles, whose thicknesses are directly proportional to the thicknesses of the hypabyssal bodies and vary from 20–30 cm to 5–7 m. No outer contact aureoles were found around the granite-aplite sills.

METHODS

Our research is based on the results obtained on 22 samples of hypabyssal rocks from the Omgon Range (see Fig. 2c for sampling sites).

Individual zircon and apatite grains from titanomagnetite gabbro-dolerite and biotite granites were dated by the fission-track method (Table 1) at the Laboratory of Mineralogical and Track Analysis of the Geological Institute, Russian Academy of Sciences, with the use of an external detector (Wagner and Van den Haute, 1992).

All of the samples were examined petrographically, and their minerals were analyzed (Tables 2–6). All rock samples were analyzed for major elements. Representative samples were additionally analyzed for trace elements by ICP-MS (Table 7), and other samples were analyzed for these elements by XRF (these analyses are not listed in this publication). Rb–Sr isotopic data were obtained on six whole-rock samples (Table 9). In order to simulate the magmatic processes, the concentrations of trace elements were determined by the inductively coupled plasma mass-spectrometry (Table 8), and the Rb and Sr isotopic compositions (Table 9) were analyzed in three and two samples, respectively, of the terrigenous rocks hosting the hypabyssal intrusions.

Minerals were analyzed at the laboratory of the Geological Faculty of the Moscow State University on a Camscan-4DV scanning electron microscope (analyst N.N. Karotaeva). The compositions of minerals and the groundmass of the rocks were determined on a Link AN-10000 EDS analytical setup at an accelerating voltage of 15 kV and a beam current of 1–3 nA. The detection limits of elements were (wt %): >0.12 for K_2O, >0.15 for SiO_2, >0.18 for Al_2O_3 and TiO_2, >0.20 for FeO, MnO, MgO, CaO, and Cr_2O_3, and >0.5 for Na_2O. The analyses were conducted at analytical spots with X-ray radiation generated within an area of approximately 3 μm in diameter. Inasmuch as the beam current was not stabilized, the analytical totals could not be used as a criterion of the quality of the analyses and were automatically normalized to 100 wt % (Table 2–6). The quality of the analyses was estimated using the fit indices and from stoichiometric considerations, using the calculated cation proportions of the minerals.

Major elements were determined by XRF on a VRA-20R X-ray analyzer at the Institute of Mineralogy

Table 1. Fission-track age of zircon and apatite from sills of the Omgon Range

Sample	Mineral	ρs	Ns	ρi	Ni	ρd	*n*	χ^2	Age	−1σ	+1σ	U ± 2σ
O-27	Zircon	6.85	1766	5.03	1296	2.65	30	99.4	62.5	−3.3	+3.5	231.0 ± 17.8
O-27	Apatite	0.45	222	1.12	551	29.3	15	100.0	60.9	−6.7	+7.6	15.2 ± 1.4
O-43	Zircon	10.5	1116	8.42	891	2.92	17	100.0	63.0	−3.8	+4.0	350.9 ± 32.7

Note: ρs is the density ($cm^{-2} \times 10^{-6}$) of ^{238}U spontaneous fission tracks; Ns is the counted number of spontaneous fission tracks; ρi is the density ($cm^{-2} \times 10^{-6}$) of ^{238}U-induced fission tracks; ρd is the density ($cm^{-2} \times 10^{5}$) of fission tracks in the fluence monitor (low-U mica); *n* is the counted number of grains; χ^2 is the Chi-squared probability (%). The age values are integrated. The Zeta factor of zircon was calculated using eight age standards (Fish Canyon Tuff and Buluk Tuff) and equals 348.2 ± 11.02 (±1σ) (Hurford, 1998). The Zeta factor of apatite is based on seven determinations (Fish Canyon Tuff and Buluk Tuff) and equals 104.32 ± 3.35 (±1σ)(Hurford, 1998). The samples were irradiated at the Oregon State University Nuclear Reactor with a nominal fleunce of approximately 2×10^{15} neutron/cm^2 for zircon and 8×10^{15} neutron/cm^2 for apatite. U-doped glass standards (CN-5 for zircon and CN-1 for apatite) were placed at either the end of the sample stack (to monitor fluence during irradiation). The fluence gradient was calculated using the glasses, and the extrapolated values were utilized to calculate the age. All samples were counted at a magnification of 1562.5^x under an Olympus BH-P microscope with a dry objective, an automated stage, and a digitizing tablet. *U* is the U content in ppm (±2σ). Age values are given in Ma.

and Petrography, Siberian Division, Russian Academy of Sciences, using conventional methods of sample preparation and analysis. Trace elements were analyzed by ICP-MS on a PerkinElmer/SciexElan 6100 DRC mass spectrometer at the Institute of Mineralogy, Geochemistry, and Crystal Chemistry of Rare Elements (analyst D.Z. Zhuravlev). Samples were prepared for the analysis by a method involving decomposition in acid. The Rb–Sr isotopic data on whole-rock samples of the hypabyssal magmatic rocks and their host terrigenous rocks were measured on a Finnigan MAT-262 mass spectrometer at the Institute of Mineralogy, Geochemistry, and Crystal Chemistry of Rare Elements (analyst V.S. Bogatov), using conventional techniques of sample preparation and analysis.

AGE OF HYPABYSSAL ROCKS FROM THE OMGON RANGE

The Early Paleocene age of hypabyssal rocks in the Omgon Range was confirmed by fission-track dates of apatite and zircon (Table 1). The fission-track zircon age of the titanomagnetite gabbro-dolerite is 62.5 ± 3.4 Ma, and that of the biotite granite is 63.0 ± 4.0 Ma. Apatite age from the same gabbro-dolerite sample is also close to these values: 60.9 ± 7.2 Ma. Although the fission-track dates of the zircon and apatite correspond to the cooling age of these minerals to approximately 215–240°C (Brandon and Vance, 1992) and ~111 ± 6°C (Laslett *et al.*, 1987), respectively, the aforementioned dates are close to the emplacement time of the rocks, because (i) the hypabyssal rocks crystallized at relatively shallow depths (<4 km, according to geothermometric evidence, see below), and (ii) the apatite age of sandstone from the Omgon Group (this age was reset during the thermal event, perhaps, under the effect of the mafic magma) is 57.7 ± 7.0 Ma (Sobolev *et al.*, 2005) and is close, within the error, to the apatite age of the biotite granite.

PETROGRAPHY

The **gabbro-dolerites** with microgranitic and micrographic textures of their groundmass are ilmenite and titanomagnetite varieties with similar rock fabrics. The central portions of the hypabyssal bodies consist of these rocks with patches of micropoikilitic and microphitic textures (which will be referred to below as dolerite patches), with the space in between filled with quartz, orthoclase, and, more rarely, albite and micrographic (granophyric) aggregates of quartz + albite ± orthoclase (which will be referred to below as the groundmass). The chill zones typically consist of glomerophyric and porphyritic rocks. Dolerite patches account for 70–75 to 90% of thin sections by area. The titanomagnetite gabbro-dolerites are richer in ore minerals than the ilmenite gabbro-dolerites.

Dolerite patches with micropoikilitic and microphitic textures consist of zonal clino- and orthopyroxene grains (Table 2) or serpentine ± chlorite + magnetite pseudomorphs after these minerals, often with saussuritized zonal plagioclase grains of bytownite–labradorite or andesine–oligoclase composition (Table 3), pseudomorphs of chlorite with disseminated magnetite after biotite, and pale green chlorite and amphibole of tremolite–actinolite composition. The accessory minerals in dolerite patches are skeletal grains of ilmenite or euhedral titanomagnetite grains with ilmenite exsolution lamellae (Table 4) and sphene.

Plagioclase occurs as tabular crystals and randomly oriented elongated laths, which are mostly included in clinopyroxene grains that have variable sizes and subhedral prismatic shapes. The opposite relations were observed in sample O-29 (ilmenite gabbro-dolerite), in which an inclusion of high-Mg augite (Table 2) was found in a labradorite grain (Table 3). Pseudomorphs after biotite usually develop around Fe and Ti oxide minerals and clinopyroxene. Pale green chlorite and tremolite–actinolite fill the interstitial space between plagioclase and pyroxene grains. In the rocks with

Table 2. Representative analyses (wt %) of pyroxenes in hypabyssal rocks from the Omgon Range

Component	O-29[1]*						O-29(1)		
	Mg*Aug*[2]*		*Aug*	Fe*Aug*	*Br*	*Hy*	Mg*Aug*	Fe*Aug*	*Sal*
	1[3]*		2	3	2		1	2	3
	1[4]*	2			3	4	5		
	incl. in *Pl*	core	margin	rim	core	core	core	margin	rim
SiO_2	52.85	52.87	51.64	51.02	53.63	52.77	52.26	50.05	52.23
TiO_2	0.53	0.54	0.61	0.29	0.64	0.48	0.49	0.27	0.35
Al_2O_3	1.99	2.35	1.29	0.41	0.97	0.72	2.36	0.32	0.64
FeO	5.82	5.00	11.97	18.44	17.05	21.40	5.53	19.56	8.73
MnO	–	0.22	0.21	0.28	0.33	0.46	–	0.36	0.31
MgO	16.61	16.75	13.95	8.74	25.35	21.86	17.30	9.94	14.46
CaO	21.42	20.91	19.59	20.09	1.68	1.87	20.62	18.50	22.55
Na_2O	–	–	–	0.63	–	–	–	0.60	–
K_2O	–	–	–	–	–	–	–	–	0.12
Cr_2O_3	0.48	0.89	–	–	–	–	0.75	–	–
NiO	–	–	0.21	–	–	–	–	–	–
Mg#	83.57	85.66	67.52	46.03	72.61	64.55	84.78	47.54	74.70
	6(O)								
Si^{4+}	1.940	1.936	1.936	1.977	1.952	1.970	1.910	1.938	1.945
Al^{3+}(IV)	0.060	0.064	0.064	0.023	0.048	0.030	0.090	0.062	0.055
Al^{3+}(VI)	0.026	0.037	–	–	–	0.001	0.012	–	–
Ti^{4+}	0.015	0.015	0.017	0.009	0.018	0.014	0.013	0.008	0.010
Fe^{2+}	0.179	0.153	0.303	0.536	0.487	0.671	0.112	0.490	0.183
Fe^{3+}	0.000	0.000	0.072	0.061	0.032		0.057	0.144	0.089
Mn^{2+}	–	0.007	0.007	0.009	0.010	0.015	–	0.012	0.010
Mg^{2+}	0.909	0.914	0.780	0.505	1.376	1.216	0.942	0.574	0.803
Ca^{2+}	0.842	0.820	0.787	0.834	0.066	0.075	0.807	0.767	0.900
Na^{+}	–	–	–	0.047	–	–	–	0.045	–
K^{+}	–	–	–	–	–	–	–	–	0.005
Cr^{3+}	0.014	0.026	–	–	–	–	0.022	–	–
Ni^{+}	–	–	0.006	–	–	–	–	–	–
Al_{tot}	0.086	0.101	0.057	0.018	0.042	0.032	0.102	0.014	0.028
Fe_{tot}	0.179	0.153	0.375	0.597	0.519	0.668	0.169	0.633	0.272
En	47.1	48.4	40.2	25.3	70.2	62.1	49.1	28.3	40.7
Wo	43.6	43.5	40.5	41.9	3.3	3.8	42.1	37.8	45.6
Fs	9.3	8.1	19.3	30.0	26.5	34.1	8.8	31.2	13.8
Ac	–	–	–	2.4	–	–	–	2.2	–
T, °C	–	1100	–	–	–	–	1100	–	450
P, kbar	–	3.5	–	–	–	–	3.8	–	0.5

Table 2. (Contd.)

Component	O-29(2)			O-38			O-40		
	Aug	*Aug*	*Aug*	*Aug*		*Hy*	*Aug*		Fe*Aug*
	1	2	3	1	2		1	2	3
	6		7	8		9	10		
	core	margin	core	core	margin	core	core	margin	rim
SiO_2	52.66	50.90	50.98	51.43	51.55	51.18	51.41	51.38	51.30
TiO_2	0.58	0.44	–	0.93	0.48	–	0.76	0.52	–
Al_2O_3	1.66	1.04	0.95	2.01	1.30	0.30	1.52	1.03	0.31
FeO	8.38	16.63	15.79	11.21	13.19	27.93	11.96	14.72	18.96
MnO	–	0.23	0.41	0.48	0.43	0.87	0.48	0.49	0.50
MgO	16.18	11.93	10.06	13.51	12.74	16.23	13.50	12.28	8.99
CaO	19.92	18.43	20.73	20.05	19.94	3.10	19.53	18.99	19.17
Na_2O	–	–	0.58	–	–	–	–	–	0.61
K_2O	–	–	–	–	–	–	–	0.09	–
Cr_2O_3	–	–	–	–	0.13	–	–	–	–
NiO	–	–	–	–	–	–	0.38	–	–
Mg#	77.50	56.11	53.17	68.25	63.27	50.88	66.81	59.80	45.80
	6(O)								
Si^{4+}	1.946	1.947	1.956	1.932	1.950	1.974	1.934	1.955	1.989
Al^{3+}(IV)	0.054	0.053	0.044	0.068	0.050	0.026	0.066	0.045	0.011
Al^{3+}(VI)	0.019	–	–	0.020	0.007	–	0.001	0.002	0.003
Ti^{4+}	0.016	0.013	–	0.026	0.014	–	0.022	0.015	0.000
Fe^{2+}	0.245	0.487	0.434	0.334	0.388	0.851	0.332	0.436	0.562
Fe^{3+}	0.014	0.045	0.073	0.018	0.030	0.050	0.044	0.033	0.053
Mn^{2+}	–	0.007	0.013	0.015	0.014	0.028	0.015	0.016	0.016
Mg^{2+}	0.892	0.680	0.575	0.756	0.718	0.933	0.757	0.697	0.519
Ca^{2+}	0.789	0.755	0.852	0.807	0.808	0.128	0.787	0.774	0.796
Na^{+}	–	–	0.043	–	–	–	–	–	0.045
K^{+}	–	–	–	–	–	–	–	0.004	–
Cr^{3+}	–	–	–	–	0.004	–	–	–	–
Ni^{+}	–	–	–	–	–	–	0.011	–	–
Al_{tot}	0.072	0.047	0.043	0.089	0.058	0.014	0.067	0.046	0.014
Fe_{tot}	0.259	0.532	0.507	0.352	0.417	0.901	0.376	0.469	0.615
En	34.6	46.4	28.9	39.5	40.4	47.6	39.5	39.4	26.1
Wo	38.4	40.9	42.8	42.1	41.5	6.5	41.2	41.0	40.0
Fs	27.0	12.7	25.5	18.4	18.1	45.9	19.3	19.6	30.9
Ac	–	–	2.2	–	–	–	–	–	2.3
T, °C	1080	–	–	–	–	–	1000	1000	–
P, kbar	5.9	–	–	–	–	–	3.2	2.2	–

Note: [1]* Sample numbers here and in Tables 3–8; [2]* mineral here and in Table 4: *Cpx*—clinopyroxene, Mg*Aug*—high-Mg augite, *Aug*—augite, Fe*Aug*—ferroaugite, *Sal*—salite, Fe*Sal*—ferrosalite, *Hy*—hypersthene, *Br*—bronzite; [3]* associations here and in Tables 3, 4: (**1**) clinopyroxenes that crystallized in deep magma chambers from mafic magmas under pressures of 7–2 (±2) kbar; (**2**) pyroxenes that crystallized in sills from mafic magmas; (**3**) clinopyroxenes that crystallized from mafic magmas contaminated by acid melts; [4]* grain numbers here and in Tables 3–5; dashes mean concentrations below the detection limits. The cation proportions were calculated following (Morimoto, 1989). The crystallization temperatures of pyroxenes were evaluated by geothermometers (Wells, 1977; Wood and Banno, 1973; Lindsley, 1983); the pressures were calculated accurate to ± 2 kbar by the geobarometer (Nimis, 1995). The occurrence or absence of equilibrium between coexisting ortho- and clinopyroxene were tested following the method (Nakamura and Kushiro, 1970; Hunter, 1998).

Table 3. Representative analyses (wt %) of plagioclase in hypabyssal rocks from the Omgon Range

Component	O-29[1]*						O-29(1)					
	1[3]*		2				1		2		3	
	1	2	3		4	5	6	7	8	9	10	
	core	core	core	margin	core	core	core	core	core	core	core	margin
SiO_2	51.99	50.85	51.99	53.84	50.20	54.10	48.80	52.17	49.68	53.96	55.61	66.81
Al_2O_3	30.00	30.49	29.41	28.53	30.99	27.72	31.59	29.60	31.20	28.39	27.26	20.06
FeO	0.40	0.28	0.55	0.59	0.31	0.56	0.54	0.44	0.52	0.37	0.63	0.64
CaO	13.60	14.19	13.32	12.06	14.98	12.18	15.78	13.14	14.97	11.65	10.28	1.87
Na_2O	3.72	3.50	4.05	4.58	2.99	4.88	2.74	4.08	3.00	4.91	5.75	9.32
K_2O	0.10	0.21	0.18	0.16	0.15	0.22	0.14	0.14	0.18	0.22	0.33	1.14
An	66.5	68.3	63.9	58.7	72.9	57.2	75.5	63.5	72.7	56.0	48.8	9.3
Ab	32.9	30.5	35.1	40.4	26.3	41.5	23.7	35.7	26.3	42.7	49.4	84.0
Or	0.6	1.2	1.0	0.9	0.9	1.2	0.8	0.8	1.0	1.2	1.8	6.7

Component	O-40					O-27				
	1			2						
	11	12			13	14				15
	core	core	i.z.	core	core	core	i.z.	i.z.	margin	core
SiO_2	53.69	55.34	55.32	58.86	62.01	60.20	63.46	61.29	66.53	58.35
Al_2O_3	28.72	27.75	27.37	25.63	23.77	24.52	21.68	23.99	21.10	25.98
FeO	0.52	0.73	0.80	0.37	0.43	0.23	0.79	0.09	0.17	0.14
CaO	11.74	10.64	10.46	7.96	5.54	6.78	5.00	6.16	2.06	8.20
Na_2O	4.85	5.14	5.56	6.34	7.52	7.06	6.07	7.44	9.90	6.71
K_2O	0.19	0.16	0.19	0.57	0.50	0.72	1.61	0.80	0.12	0.40
An	56.6	52.9	50.4	39.5	28.1	33.2	27.9	30.0	10.2	39.4
Ab	42.3	46.2	48.5	57.1	68.9	62.6	61.3	65.4	89.1	58.3
Or	1.1	1.0	1.1	3.4	3.0	4.2	10.7	4.6	0.7	2.3

Note: Abbreviations: i.z.—intermediate zone. Grains 1, 2, 6, 7, 11 are poikilitic inclusions in clinopyroxenes of Generation I; (3–5) and (8–13) are tabular crystals; (14) megacryst; (15) lath in groundmass.

glomeroporphyritic and porphyritic textures, plagioclase occurs as aggregates of broad, optically unzoned tabular grains and as clearly zoned elongated crystals, with interstices filled with plagioclase laths of calcic and intermediate composition, clinopyroxene, and pale green chlorite.

The groundmass of the gabbro-dolerites consists of quartz, orthoclase, albite, and micrographic aggregates of these minerals, whose outlines are controlled by the morphology of the dolerite patches. In large interstices, the texture of the groundmass is clearly hypidiomorphic-granular (microgranitic). The accessory minerals in the groundmass of the gabbro-dolerites are zircon, apatite, and much more rare ilmenite.

The **quartz microdiorite** consists of large euhedral phenocrysts of zonal saussuritized (or, in places, chloritized) plagioclase and glomerophyric aggregates of plagioclase with clinopyroxene or, more rarely, plagioclase, clinopyroxene, and pseudomorphs of serpentine + magnetite or serpentine + chlorite + disseminated magnetite after orthopyroxene and chlorite + magnetite pseudomorphs after biotite. The phenocrysts and their aggregates are submerged in a groundmass of granitic and micrographic texture. The rocks contain from 50–70 to 30–40% phenocrysts and glomerophyric aggregates (counted by area in thin sections). The texture of the glomerophyric aggregates resembles that of the plagioclase-phyric dolerites, in which plagioclase occurs as large euhedral zonal crystals and clinopyroxene forms anhedral prismatic grains in between. The glomerophyric aggregates contain single ilmenite grains.

The groundmass consists of aggregates of anhedral quartz and orthoclase grains and micrographic aggregates of quartz + albite ± orthoclase that penetrate feld-

Table 4. Composition (wt %) of ilmenite and titanomagnetite in hypabyssal rocks from the Omgon Range

Component	O-29[1]*			O-29(1)	O-29(2)		O-29(4)	O-38			
	Ilm[2]*	*Ilm*	*Ilm*	*Ilm*	*Ilm*	*Ilm*	*Ilm*	*Ilm*	*TiMt*	*Ilm*	*Ilm*
	1[3]*	2	3	4	5	6	7	8	9	10	11
TiO_2	51.95	50.65	51.31	51.04	49.94	50.06	51.10	49.75	13.45	49.58	49.57
Al_2O_3	–	–	–	–	–	–	–	–	1.71	–	–
FeO	46.19	48.36	45.08	47.81	48.66	48.47	46.21	49.00	82.86	49.05	49.45
MnO	1.34	–	2.95	0.34	0.48	0.67	1.47	0.29	0.33	0.38	0.37
MgO	–	0.28	–	–	–	0.34	–	0.58	–	0.40	0.24
Total	99.48	99.30	99.34	99.19	99.07	99.54	98.78	99.62	98.34	99.41	99.63
FeO	37.74	37.56	35.50	37.88	36.79	36.42	36.99	36.31	36.91	36.21	36.29
Fe_2O_3	9.39	12.00	10.64	11.03	13.19	13.40	10.25	14.10	51.06	14.27	14.62
Ilmenite	95.40	95.00	89.60	96.10	92.80	91.90	94.10	94.10	–	91.70	92.20
Pyrophanite	2.90	0.30	6.40	0.70	1.00	1.40	3.20	0.60	–	0.80	0.80
Geikielite	0.50	1.10	0.60	0.50	0.00	1.30	0.00	2.20	–	1.50	0.90
Hematite	1.20	3.60	3.40	2.70	6.10	5.30	2.70	5.90	–	6.00	6.10
T, °C[5]*	–	–	–	–	–	–	–	–	765		
$\log f_{O_2}^{5}$*	–	–	–	–	–	–	–	–	–15.342		
T, °C[6]*	–	–	–	–	–	–	–	–	745		
$\log f_{O_2}^{6}$*	–	–	–	–	–	–	–	–	–15.901		

Component	O-40										O-33
	TiMt	*Ilm*	*TiMt*	*Ilm*	*TiMt*	*Ilm*	*TiMt*	*Ilm*	*TiMt*	*Ilm*	*Ilm*
	12	13	14		15		16		17		18
TiO_2	12.96	50.08	13.79	50.08	17.28	50.41	13.17	49.90	13.79	50.53	50.74
Al_2O_3	0.45	–	0.64	–	0.61	–	0.65	–	0.49	–	–
FeO	85.58	47.93	84.02	47.15	80.90	48.38	85.04	48.79	84.19	47.97	47.79
MnO	0.23	0.59	0.36	0.60	0.50	0.65	0.30	0.57	0.53	0.74	0.85
MgO	-	0.56	–	0.48	-	0.37	0.06	0.29	0.18	0.37	0.33
Total	99.21	99.16	98.80	98.31	99.28	99.81	99.20	99.55	99.17	99.61	99.70
FeO	36.92	36.39	37.53	36.55	40.58	36.72	36.99	36.39	37.58	36.78	36.89
Fe_2O_3	54.07	12.83	51.67	11.78	44.80	12.96	53.39	13.78	51.79	12.43	12.11
Ilmenite	–	89.10	–	86.80	–	92.40	–	91.70	–	92.50	92.90
Pyrophanite	–	1.30	–	1.40	–	1.40	–	1.20	–	1.60	1.80
Geikielite	–	2.20	–	1.90	–	1.40	–	1.10	–	1.40	1.30
Hematite	–	7.50	–	9.90	–	4.80	–	6.00	–	4.50	4.10
T, °C[5]*	–	–	834		794		757		733		–
$\log f_{O_2}^{5}$*	–	–	–13.18		–15.121		–15.525		–16.531		–
T, °C[6]*	–	–	824		734		737		694		–
$\log f_{O_2}^{6}$*	–	–	–13.406		–16.729		–16.041		–17.722		–

Note: *TiMt*—titanomagnetite, *Ilm*—ilmenite. Temperature and oxygen fugacity were evaluated following [5]*—(Powell and Powell, 1977) and [6]*—(Anderson and Lindsley, 1985).

spar grains. The groundmass contains single mica flakes. The accessory minerals are zircon, acicular and prismatic apatite, and ilmenite.

The **biotite granite** is a porphyritic rock, whose large (up to 2.5 cm across) phenocrysts are zonal plagioclase grains of andesine–oligoclase composition with albite outermost parts (Table 3). The plagioclase is partly saussuritized, chloritized, and carbonatized. Other phenocrysts are anhedral quartz and, more rarely eastonite (Table 5), which is partly replaced by chlorite and magnetite. The groundmass has a micrographic texture. The accessory minerals are ilmenite, zircon, and apatite.

The **granite-aplite** contains foreign microphenocrysts and microinclusions of altered plagioclase and pyroxene (?), submerged in a groundmass of micrographic and micrographic texture. Foreign phenocrysts are surrounded by rims consisting of micrographic aggregates of quartz + albite ± orthoclase. Granophyric patches sometimes occur away from the foreign phenocrysts. The groundmass consists of euhedral and subhedral laths of sericitized plagioclase, anhedral quartz, which often occurs as aggregates of grains, sphene pseudomorphs (perhaps, after biotite), small flakes of colorless mica, and carbonate. The accessory minerals are ilmenite, zircon, and apatite.

MINERALOGY

Clinopyroxene was analyzed in the ilmenite [samples O-29 and O-29(1)] and titanomagnetite (samples O-38 and O-40) gabbro-dolerites and quartz microdiorites [sample O-29(2)]. Representative analyses of clinopyroxene are listed in Table 2. The analysis of the compositional variations in the clinopyroxene and its morphological features led us to classify this mineral into three generations: (I) high-Mg augite, (II) augite, and (III) clinopyroxene with elevated Ca concentrations, high-Ca augite, ferroaugite, and ferrosallite.

High-Mg augite (generation I) was found exclusively in ilmenite gabbro-dolerite and quartz microdiorite, in which this mineral is contained as small resorbed grains in labradorite or composes the cores of large anhedral-prismatic grains with poikilitic inclusions of bytownite and labradorite (Table 3).

High-Mg augite that was analyzed in our rock samples has a practically unchanging composition (Fig. 3a): $Wo_{43.65–41.41}En_{49.13–47.09}Fs_{10.92–7.87}$, Mg# = 86.1–81.4 (sample O-29) and $Wo_{42.93–42.07}En_{49.11–46.93}Fs_{10.38–8.81}$, Mg# = 84.78–81.89 [sample O-29(1)]. The mineral is low-Al (1.71–2.36 wt % Al_2O_3), moderate-Ti (0.68–0.45 wt % TiO_2), low-Na (<0.5 wt % Na_2O) pyroxene with somewhat elevated Cr contents (0.89–0.74 wt % Cr_2O_3). The quartz microdiorite [sample O-29(2)] contains slightly more evolved varieties: $Wo_{40.93–39.78}En_{46.36–38.54}Fs_{21.68–12.71}$, Mg# = 78.48–74.44. The minerals are weakly zonal (normal zoning), with a slight decrease in the Mg# and Al content from cores to peripheries and a more significant decrease in the Cr_2O_3 and an increase TiO_2 concentrations.

Augite (generation II) dominates among the clinopyroxenes and was found in all of the analyzed samples. The mineral occurs as rims overgrowing cores of

Table 5. Composition (wt %) of biotite from a granite porphyry sill in the Omgon Range

Component	O-27[1]*	
	1[4]*	2
	incl. in *Pl* megacryst	
SiO_2	36.215	36.438
TiO_2	5.365	4.720
Al_2O_3	17.326	16.666
FeO	19.491	19.467
MgO	11.381	13.038
Na_2O	0.525	0.437
K_2O	9.261	8.681
Si^{2+}	2.64	2.65
Al^{3+}(IV)	1.36	1.35
Al^{3+}(VI)	0.13	0.08
Fe^{3+}	0.44	0.60
Ti^{4+}	0.29	0.26
Mg^{2+}	1.24	1.41
Fe^{2+}	0.75	0.59
Na^{+}	0.07	0.06
K^{+}	0.86	0.81
Mg#	0.51	0.54

Table 6. Integral composition (wt %) of granophyre patches in hypabyssal rocks of the Omgon Range

Component	O-29[1]*	O-29(2)	O-29(4)	O-40	O-33
	$N = 1$	$N = 2$	$N = 2$	$N = 3$	$N = 3$
SiO_2	79.91	75.18	76.31	78.56	78.69
TiO_2	–	0.16	–	0.06	0.19
Al_2O_3	11.36	12.76	11.45	11.16	10.28
FeO	0.23	1.06	1.18	0.68	0.69
MnO	–	0.10	0.01	0.00	0.02
MgO	–	0.39	0.17	0.14	0.12
CaO	0.92	1.05	1.97	0.63	0.72
Na_2O	4.44	4.89	3.50	3.09	1.07
K_2O	2.43	3.84	4.31	5.08	7.29
Cr_2O_3	0.41	0.38	0.62	0.51	0.93

Note: N is the number of measurements.

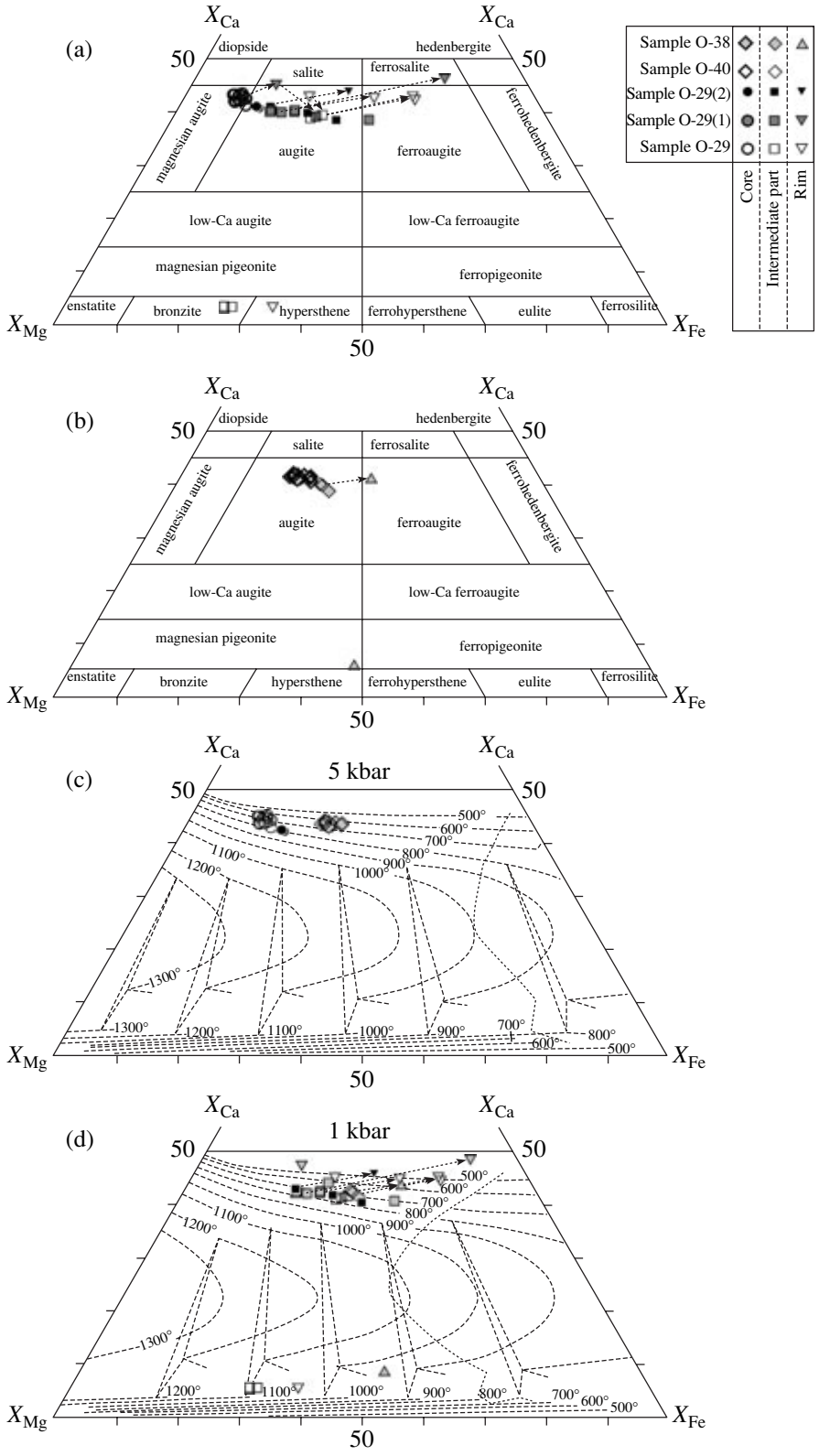

Fig. 3. Ternary $(Ca,Mg,Fe^{2+})Si_2O_6$ classification diagram for pyroxenes from Lower Paleocene hypabyssal rocks of the Omgon Range and the evaluated crystallization temperatures of these pyroxenes.

(a) Pyroxenes of the ilmenite gabbro-dolerites and quartz microdiorites; (b) pyroxenes of the titanomagnetite gabbro-dolerites; (c) estimated crystallization temperatures of high-pressure clinopyroxene (generation I); (d) estimated crystallization temperatures of low-pressure clinopyroxene (generations II and III). Isotherms of pyroxenes are compiled from (Lingsley, 1983).

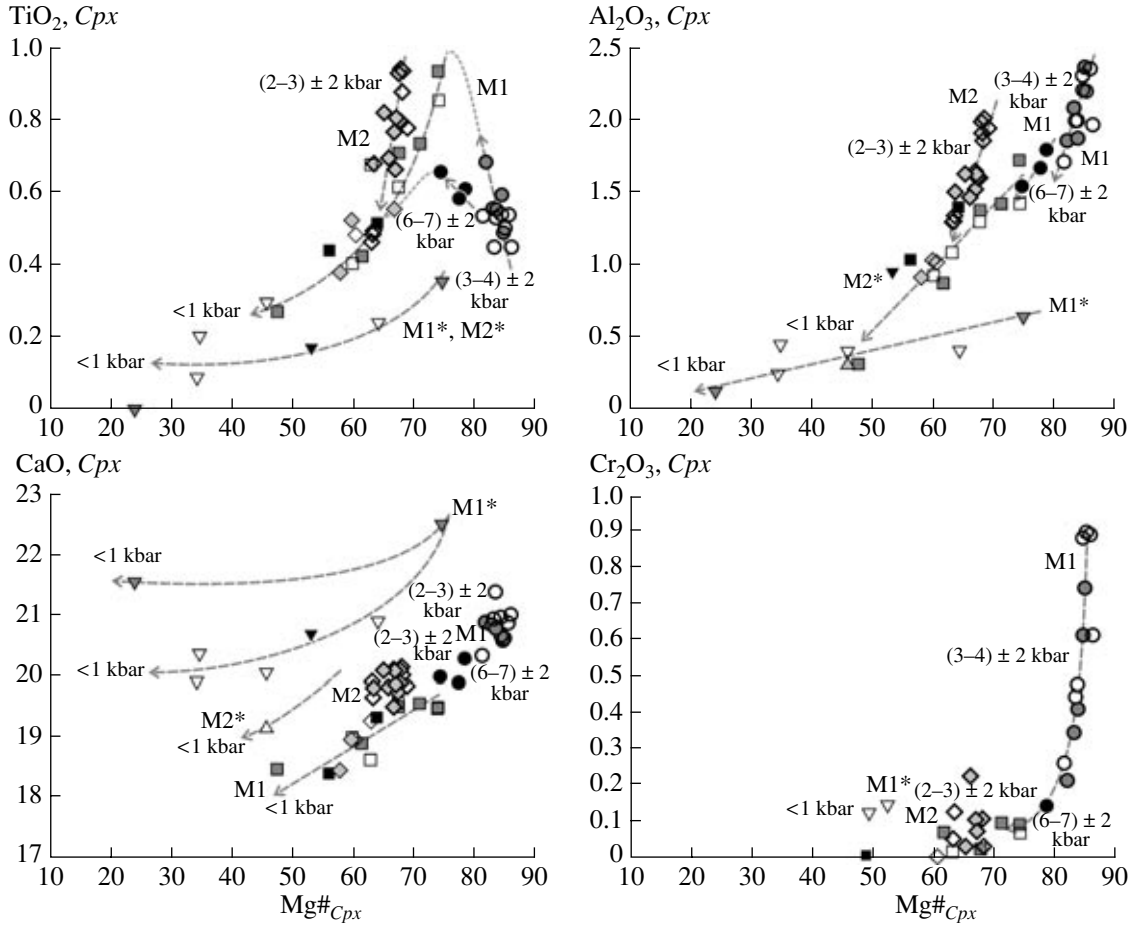

Fig. 4. Correlation between the Mg mole fraction of clinopyroxene ($Mg\#_{Cpx}$) and concentrations (wt %) of elements in this mineral. The diagrams demonstrate the compositional evolution of clinopyroxene during its crystallization in mafic magmas uncontaminated by rhyolite melts (*M1*, *M2*) and mafic magma contaminated with rhyolitic melts (*M1**, *M2**). *M1* and *M1** are the magmas whose crystallization products are ilmenite gabbrodolerites, and *M2* and *M2** are the magmas whose crystallization products are Ti–Mt gabbrodolerites and quartz microdiorites. See Fig. 3 for symbol explanations.

high-Mg augite in the central parts of grains or composes individual anhedral grains with poikilitic inclusions of bytownite and labradorite.

Augites from the ilmenite gabbro-dolerites have practically identical compositions, which vary within broad ranges. The mineral has the composition $Wo_{40.53–39.01}En_{44.32–36.21}Fs_{24.18–15.48}$ in sample O-29 and $Wo_{40.53–39.34}En_{44.03–37.32}Fs_{23.34–15.44}$ in sample O-29(1). Augite from the titanomagnetite gabbro-dolerites shows narrower compositional variations: $Wo_{42.13-40.10}En_{40.36–36.22}Fs_{23.68–18.15}$ in sample O-38 and $Wo_{42.01–38.79}En_{39.72–35.45}Fs_{25.76–18.63}$ in sample O-40 (Fig. 3a).

In a $Mg\#_{Cpx}$ vs. TiO_2 and $Mg\#_{Cpx}$ vs. Al_2O_3 diagrams (Fig. 4), augites from the ilmenite and titanomagnetite rocks define distinct trends. Augite from both groups of the gabbro-dolerites displays similar tendencies in the compositional evolution. The mineral has a clearly pronounced normal zoning, with Mg# decreasing from cores to margins and the CaO, Al_2O_3, and TiO_2 contents simultaneously decreasing at an increase in the FeO concentrations.

High-Ca clinopyroxene: salite, ferrosalite, high-Ca augite, and high-Ca ferroaugite (generation III) was found in the ilmenite and titanomagnetite gabbro-dolerites, in which it occurs as the outermost parts of grains of high-Mg augite and augite in contact with groundmass minerals.

High-Ca clinopyroxene is the most diverse in composition, perhaps, because of variations in the composition of the seed grains (Figs. 3a, 3b, 4). The common chemical feature of these minerals is their significant enrichment in the Ca end member (Figs. 3a, 3b, 4) compared to the high-Mg augite and augite, a fact supposedly reflecting a drastic increase in the alkalinity of the melt.

Orthopyroxene was analyzed only in two gabbro-dolerite samples, because this mineral is highly susceptible to replacement by serpentine ± chlorite + magnetite. Representative analyses of orthopyroxene are presented in Table 2. The mineral corresponds to bronzite

$Wo_{3.71–3.35}En_{70.18–68.79}Fs_{27.57–26.29}$ in sample O-29 (ilmenite gabbro-dolerite) and to hypersthene $Wo_{6.53–3.82}En_{62.08–47.56}Fs_{45.91–34.09}$ in samples O-29 (ilmenite gabbro-dolerite) and O-38 (titanomagnetite gabbro-dolerite).

The mineral is weakly zoned, but its composition significantly varies even within a single sample: Mg# = 72.69–64.55 and 50.88. As the Mg# of the mineral decreases, its SiO_2, TiO_2, and Al_2O_3 concentrations also decrease and the CaO and FeO contents, conversely, increase. The variations in the chemistry of the orthopyroxene are compatible with its crystallization from a mafic melt, together with plagioclase, ilmenite, and/or titanomagnetite, and augite.

The **feldspars** of the rocks are plagioclase and orthoclase. Plagioclase was analyzed in the ilmenite [samples O-29 and O-29(1)] and titanomagnetite (samples O-38 and O-40) gabbro-dolerites and biotite granites (sample O-27). Representative analyses of the plagioclase are given in Table 3. The chemical variations in this mineral in the gabbro-dolerites and its textural position in the rocks allowed us to distinguish three generations of this mineral in the dolerite patches: (I) bytownite–labradorite in association with high-Mg augite, (II) bytownite-labradorite in association with augite, and (III) andesine-oligoclase in association with high-Ca clinopyroxene. The groundmass of the gabbro-dolerites and biotite granites typically contains albite and orthoclase.

Plagioclase of *bytownite–labradorite composition (generation I)* was found only in the ilmenite gabbro-dolerites [samples O-29 and O-29(1)], in which this mineral occurs as poikilitic inclusions in high-Mg augite and euhedral grains containing resorbed grains of high-Mg augite. The anorthite concentration in this plagioclase ranges from 75.5 to 63.5.

Plagioclase of *bytownite–labradorite composition (generation II)* is contained in both the ilmenite and the titanomagnetite rocks, in which it either composes poikilitic laths in the augite cores of large clinopyroxene grains or forms individual euhedral crystals. The plagioclase of the ilmenite gabbro-dolerites [samples O-29 and O-29(1)] is richer in anorthite ($An_{72.9–56.0}$) than this mineral in the titanomagnetite varieties (sample O-40, $An_{56.6–49.1}$) with lower SiO_2 contents. Plagioclase of bytownite–labradorite composition of generation II is weakly zoned in both varieties of the gabbro-dolerites. Its zoning is normal, with an insignificant decrease in the anorthite concentration from the cores to peripheries of the crystals.

Plagioclase of *andesine–oligoclase composition (generation III)* is contained in dolerite patches in the ilmenite and titanomagnetite gabbro-dolerites, in which this mineral occurs either in the outer rims of euhedral bytownite–labradorite plagioclase of generation II or forms small individual grains. The ilmenite gabbro-dolerites contain andesine and oligoclase that are more calcic than in the titanomagnetite rocks. The composition of the plagioclase is $An_{49.1–37.6}$ and $An_{39.6–28.1}$, respectively, in the ilmenite [samples O-29 and O-29(1)] and titanomagnetite (sample O-40) gabbro-dolerites.

Andesine–oligoclase megacrysts in the biotite granites have the composition $An_{39.4–27.9}$, which is similar to that of plagioclase of andesine-oligoclase composition ($An_{39.5–28.1}$) in the titanomagnetite gabbro-dolerites.

The *K–Na feldspars* are albite and orthoclase, which were found in all rock types. The minerals are contained in the gabbro-dolerites in the groundmass. In the biotite granites, albite develops as the outermost rims around andesine–oligoclase megacrysts and orthoclase composes phenocrysts. Plagioclase of albite composition is a magmatic mineral in all of the rocks, from gabbro-dolerite to granite-aplite, and its compositions are close in all of the samples analyzed: $An_{9.3}$ in the ilmenite gabbro-dolerites, $An_{7.9}$ in the titanomagnetite gabbro-dolerites, and $An_{10.2–11.2}$ in the biotite granites.

Micas are contained in all of the rocks but are commonly extensively replaced by chlorite, so that we managed to analyze biotite (Table 5) only in a single sample of the biotite granite (sample O-27). The micas analyzed in this rock correspond to eastonite, which is characterized by high contents of Ti (4.72–5.37 wt % TiO_2), is moderately ferrous [Fe/(Fe + Mg) = 0.49–0.46], and contains much Al (16.67–17.33 wt % Al_2O_3). In tectonomagmatic diagrams, the data points of biotite

Fig. 5. Variation diagrams demonstrating the affiliation of the hypabyssal rocks with three discrete rock associations. The diagrams also shows the results of simulations of the processes that produced these series.

The ilmenite and titanomagnetite gabbro-dolerites differ in the concentrations of TiO_2, Fe_2O_3, MgO, P_2O_5, Zr, and Hf at similar SiO_2 contents. The quartz microdiorites plot on the continuation of the trends of the titanomagnetite gabbro-dolerites, a fact suggesting that the rocks are genetically interrelated. The biotite granite and granite-aplites differ from both gabbro-dolerite varieties and the quartz microdiorites by Al_2O_3, Sr, Rb, Zr, and Hf concentrations and the Rb/Sr ratios (Fig. 5b). Rocks: (1) ilmenite (moderate-Fe–Ti) gabbro-dolerites; (2) titanomagnetite (high-Fe–Ti) gabbro-dolerites; (3) quartz microdiorites; (4) biotite granite; (5) granite-aplites; (6) integral compositions of the granophyres and micrographic aggregates of quartz ± orthoclase + albite.

Light gray and black lines correspond to the surmised and calculated trends. FC—fractional crystallization, AFC—combined fractional crystallization, B_1—composition of moderate-Fe–Ti basaltic melt, B_2—composition of high-Fe–Ti basaltic melt, F_1—composition of rhyolitic melt not contaminated by the terrigenous rocks of the Omgon Group, F_2—composition of rhyolitic melt contaminated by the terrigenous rocks of the Omgon Group, M1—mixing line of B_1 and F_1, M2—mixing line of B_2 and F_2, H_1—hybrid melt produced by the mixing of the moderate-Fe–Ti basaltic magma and the rhyolitic melt. FC-1 and FC-2 are the calculated lines demonstrating the compositional evolutions of melts B_1 and B_2, respectively, during their fractional crystallization.

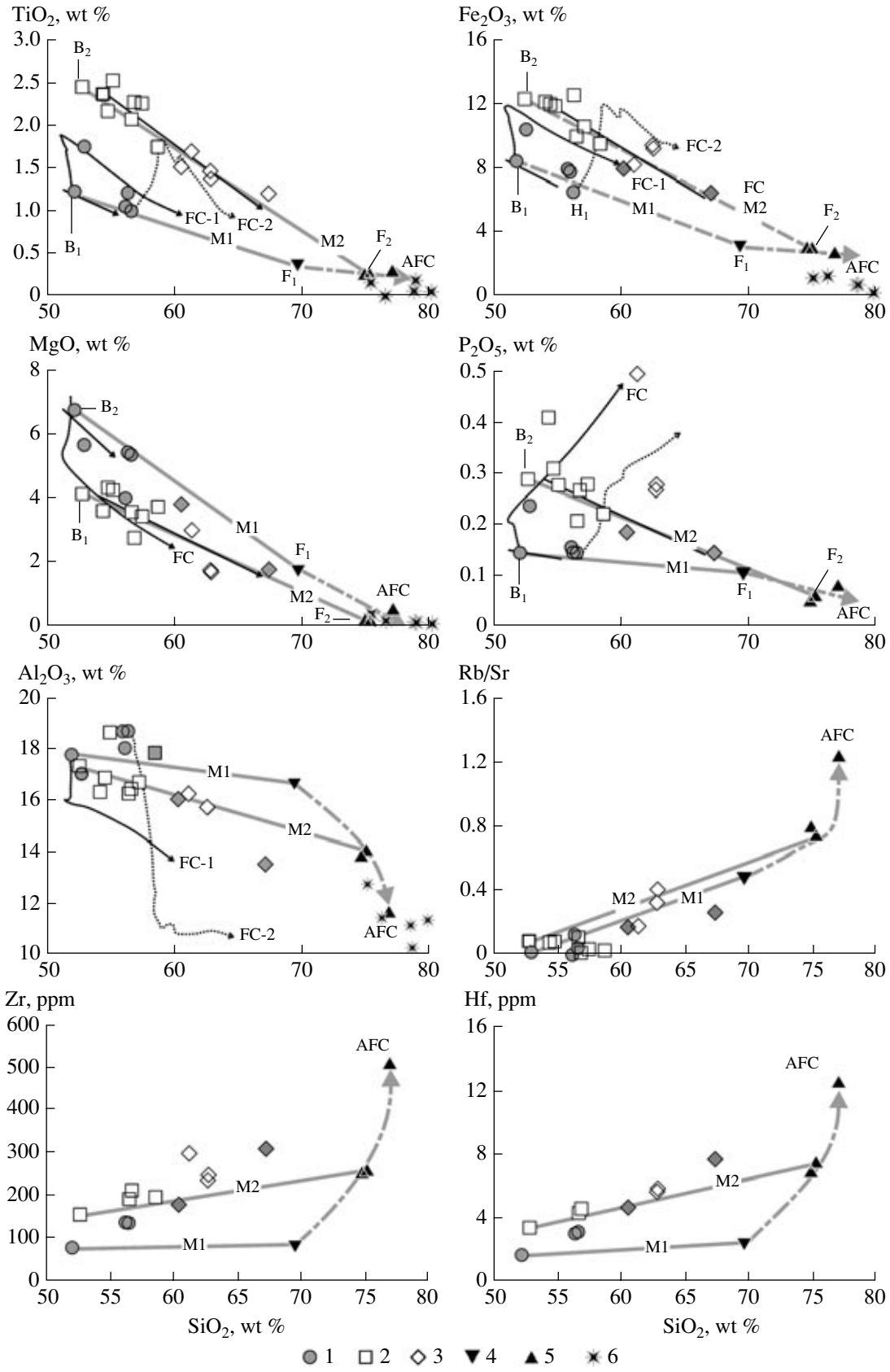
TiO2, wt %
Fe2O3, wt %
MgO, wt %
P2O5, wt %
Al2O3, wt %
Rb/Sr
Zr, ppm
Hf, ppm
B2
B1
H1
FC-1
FC-2
FC
M1
M2
F1
F2
AFC
SiO2, wt %
1 2 3 4 5 6

from the biotite granite lie within the field of micas from rocks of the calc–alkaline series.

The **ore minerals** are ilmenite and aggregates of titanomagnetite with ilmenite, which seems to be the product of the oxidation-induced exsolution of titanomagnetite. The compositions of the ore minerals are reported in Table 4. Ilmenite is typical of mafic–intermediate rocks poor in ore minerals; aggregates of titanomagnetite with ilmenite were found in rocks of mafic–intermediate composition rich in ore minerals and in the granite-aplite.

The **granophyric aggregates** consist of micrographic quartz + albite ± orthoclase and were found in all of the rocks. The integral compositions of the granophyric patches in the groundmass of the ilmenite (sample O-29) and titanomagnetite (sample O-40) gabbro-dolerites, quartz microdiorites [samples O-29(2) and O-33], and granite-aplites are listed in Table 6.

The integral compositions of the granophyric patches, which reflect the composition of the melts during the nearly eutectic crystallization of quartz, albite, and orthoclase, are similar to the compositions of the granite-aplites and plot on the continuation of the trend of the biotite granite and granite-aplite (Fig. 5). The exception is the behavior of TiO_2, Fe_2O_3, and MgO, whose contents are lower in the granophyres than in the rocks, a fact that can be explained by the concentration of these components in ilmenite, which is present in the granite-aplite but absent from the granophyre.

WHOLE-ROCK CHEMISTRY

Data on the contents of major elements, geochemistry, and isotopic composition of the hypabyssal rocks and siltstones of the Omgon Group are presented in Tables 7–9. Analysis of available data led us to distinguish three associations of the hypabyssal rocks, which define discrete trends and fields in variation diagrams (Fig. 5): (i) ilmenite gabbro-dolerites, (ii) titanomagnetite gabbro-dolerites and quartz microdiorites, and (iii) biotite granites and granite-aplites.

The **ilmenite gabbro-dolerites** petrochemically correspond to moderate-Fe–Ti, high-Al basalts and basaltic andesites of normal alkalinity (Fig. 6a). The broad scatter of the K_2O concentrations (Fig. 6b), from values typical of the rocks of the low-K tholeiitic series to those characteristic of the high-K calc–alkaline series, and the ambiguity of the reasons for these variations did not allow us to classify these rocks with any series and forced us to use other classification criteria.[1] In a FeO*/MgO–SiO_2 diagram (Fig. 6c), the data points of the ilmenite gabbro-dolerites plot along the boundary line between the tholeiitic and calc–alkaline series and highlight the dualistic nature of the rocks. Their Ta–Hf–Th relations (Fig. 8a) are close to those in basalts of the calc–alkaline series, whereas the high Ti/V ratios (up to 27.8–62.0) and the position of the data points of the ilmenite gabbro-dolerites in Ta/Yb–Th/Yb (Fig. 7) and Nb–Y–La (Fig. 8b) diagrams make these rocks quite similar to within-plate volcanics from the areas of continental and backarc rifting.

The multielement patterns of the rocks indicate that the ilmenite gabbro-dolerites are close to the basalts of volcanic arcs. These rocks are characterized by weakly fractionated chondrite-normalized (Sun and McDonough, 1989) REE patterns [$(La/Yb)_N$ = 1.53–2.67] with weak positive Eu anomalies [$Eu/Eu^* = Eu/(Sm_xGd)^{\wedge 0.5}$ = 1.24–1.06], which suggest the accumulation of small plagioclase amounts in these rocks. The least evolved sample O-56 of the ilmenite gabbro-dolerite displays a high value of its initial $(^{87}Sr/^{86}Sr)_i$ ratio, equal to 0.70532. The data on the Sr isotopic composition are consistent with the geochemical results, which indicate that the ilmenite gabbro-dolerites are enriched in LILE relative to HFSE and are significantly depleted in Nb (Nb/Nb* = 0.44–0.68) and Ta (Ta/Ta* = 0.48–0.61) (Fig. 9a). These data suggest that the parental melts could be contaminated by crustal material.

The **titanomagnetite gabbro-dolerites and quartz microdiorites** plot along the same trends and within common fields and, hence, are considered together. The titanomagnetite gabbro-dolerites correspond to Fe- and Ti-rich basalts and basaltic andesites, and the quartz microdiorites correspond to andesites, andesite-dacites, and dacites. Although the groundmass of the titanomagnetite gabbro-dolerites and quartz microdiorites contains orthoclase, the K_2O contents of these rocks and their sums of alkalis are analogous to those in rocks of normal alkalinity (Fig. 6a) belonging to the moderately-K calc–alkaline series (Fig. 6b). The only exception is sample O-50: its K_2O content is much lower, perhaps, because of the leaching of this element during biotite replacement by chlorite.

In a FeO*/MgO–SiO_2 diagram (Fig. 6c), the data points of the titanomagnetite gabbro-dolerites and quartz microdiorites plot within the field of the tholeiitic series and correspond to a trend typical of the rocks of this series. The Ti/V ratios (31.5–41.5) of the titanomagnetite gabbro-dolerites are analogous to those of basalts from continental rifting areas and rifting/spreading zones in backarc basins and mid-oceanic ridges. These rocks exhibit moderate LREE fractionation relative to HREE [$(La/Yb)_N$ = 2.00–2.07], which is similar to that in E-MORB. At the same time, the Ta–Hf–Th (Fig. 8a) and Nb–Y–La (Fig. 8b) diagrams definitely demonstrate geochemical similarities of the titanomagnetite gabbro-dolerites and quartz microdiorites to volcanics of the calc–alkaline series. These rocks are

[1] The K_2O concentrations in the ilmenite gabbro-dolerites systematically increase as the LOI values increase to 3.50 wt % and then rapidly decrease at LOI > 3.50 wt %. Considering the high mobility of K_2O and the fact that the rocks contain chlorite pseudomorphs after a dark mica (supposedly, biotite), it is highly probable that this component was removed from the rocks with high LOI values (>3.50 wt %) during low-temperature metamorphic transformations. In rocks with low LOI (<3.50 wt %), the reasons for the unsystematic variations in the K_2O contents in correlation with SiO_2 can be both low-temperature metamorphism and the presence of variable orthoclase amounts.

Table 7. Concentrations of major (wt %) and trace (ppm) elements in hypabyssal rocks of the Omgon Range

Component	O-56[1]*	O-28(6)	O-29(1)	O-38	O-31(1)	O-50	O-32	O-33	O-29(2)	O-29(3)	O-27	O-29(4)	O-31	O-34
	ilmenite gabbro-dolerite			titanomagnetite gabbro-dolerite			quartz microdiorite				biotite granite	granite-aplite		
SiO_2	50.30	54.22	54.66	51.13	54.55	53.16	60.97	60.88	58.74	65.36	67.56	75.85	73.78	73.33
TiO_2	1.19	1.17	0.97	2.39	2.01	2.14	1.34	1.43	1.48	1.17	0.35	0.30	0.28	0.26
Al_2O_3	17.24	17.45	18.16	16.90	15.75	15.46	15.33	15.33	15.65	13.18	16.21	11.55	13.87	13.63
Fe_2O_3	8.21	7.57	6.38	12.04	12.20	9.42	9.03	9.23	7.81	6.34	3.06	2.77	3.06	3.07
MnO	0.16	0.16	0.15	0.19	0.20	0.24	0.16	0.17	0.16	0.14	0.12	0.12	0.12	0.11
MgO	6.59	5.29	5.21	4.05	3.47	2.61	1.66	1.72	3.74	1.74	1.69	0.55	0.19	0.22
CaO	8.71	5.24	7.59	5.87	3.97	7.11	3.22	2.75	4.41	5.37	2.63	2.45	0.97	0.77
Na_2O	2.52	3.78	2.89	3.44	3.28	3.14	3.64	3.91	3.92	3.08	2.86	2.29	3.64	3.50
K_2O	1.72	1.53	0.75	0.94	1.01	0.31	1.68	1.56	1.27	0.79	2.71	2.72	2.29	3.24
P_2O_5	0.14	0.14	0.14	0.28	0.20	0.25	0.27	0.26	0.18	0.14	0.10	0.08	0.06	0.05
LOI	3.20	3.45	3.10	2.83	3.34	6.30	2.75	2.78	2.63	2.69	2.75	1.32	1.76	1.81
Total	99.97	100.01	99.98	100.06	99.96	100.14	100.04	100.02	99.98	100.00	100.02	99.99	100.01	100.00
Mg#	61.39	58.06	61.80	39.99	36.04	35.44	26.70	26.96	48.68	35.22	52.25	28.23	10.95	12.43
Sc	27	23	23	26	28	30	30	30	25	16	6	6	22	22
V	232	186	140	223	321	238	208	204	229	151	26	25	21	19
Cr	226	163	71	7	9	31	23	21	17	12	13	9	12	33
Mn	980	809	782	1361	1646	2369	970	1139	782	657	333	263	305	352
Co	37	29	26	28	28	28	13	12	24	15	6	4	2	2
Ni	75	90	63	11	7	24	13	11	29	14	14	10	9	16
Cu	55	33	63	34	30	76	29	26	77	113	20	32	16	17
Zn	49	90	52	92	133	86	80	93	76	61	33	27	69	67
Rb	41.3	61.2	14.0	23.5	36.0	4.5	49.4	48.4	31.7	15.8	80.1	57.7	75.5	106.1
Sr	504	481	330	271	331	344	121	148	182	60	167	46	101	132
Y	19.5	27.3	26.2	36.2	43.2	42.3	48.3	44.8	35.4	46.0	18.5	55.0	63.4	57.6
Zr	76.7	136.3	135.0	154.7	190.9	211.4	248.3	235.3	177.9	308.1	79.1	510.4	260.8	254.7
Nb	2.90	4.57	9.14	0.42	5.98	2.43	10.88	9.48	5.98	7.82	10.26	7.82	9.64	9.50
Cs	0.37	7.13	0.90	2.08	3.47	0.37	1.57	2.21	3.28	0.18	6.32	0.34	1.36	2.71
Ba	627	274	335	187	389	416	344	297	297	141	436	315	539	582
La	3.87	7.91	7.87	9.19	11.09	13.01	19.91	19.06	10.65	15.99	12.88	17.94	25.96	26.35
Ce	11.88	19.42	20.11	23.09	29.51	32.39	49.36	45.99	25.27	38.79	27.55	46.44	61.75	63.99
Pr	1.97	2.87	2.93	3.40	4.26	4.44	6.36	5.79	4.13	5.31	3.18	6.17	8.10	7.76
Nd	7.37	13.07	11.69	17.79	18.43	21.31	25.93	25.06	17.25	21.76	13.85	21.77	31.79	31.54
Sm	2.37	3.14	3.04	4.79	5.33	6.00	6.94	6.39	3.96	5.47	3.25	5.88	7.32	8.25
Eu	1.10	1.17	1.23	2.03	1.69	1.87	1.78	1.65	1.54	1.46	0.53	0.68	0.94	0.83
Gd	3.18	3.62	3.57	5.35	6.33	6.29	7.77	6.88	4.73	6.32	2.99	7.14	8.22	8.79
Tb	0.48	0.59	0.59	0.92	1.10	1.11	1.31	1.18	0.71	1.07	0.53	1.25	1.40	1.57
Dy	2.88	4.13	3.71	5.99	6.54	6.75	7.47	7.12	5.64	6.64	3.29	7.87	9.47	9.21
Ho	0.68	0.88	0.79	1.29	1.48	1.53	1.74	1.65	1.11	1.52	0.72	1.92	2.10	2.22
Er	1.93	2.24	2.25	3.30	4.22	4.22	5.06	4.63	2.66	4.28	1.86	5.92	6.01	6.62
Tm	0.27	0.37	0.36	0.48	0.61	0.57	0.70	0.64	0.50	0.67	0.27	0.88	0.96	0.90
Yb	1.76	2.08	2.05	3.07	3.84	3.88	4.56	4.31	2.56	4.08	1.77	5.67	5.76	6.07
Lu	0.27	0.32	0.32	0.43	0.59	0.57	0.72	0.63	0.39	0.65	0.25	0.96	0.89	0.92
Hf	1.95	3.30	3.40	3.67	4.59	4.87	6.12	5.93	4.94	7.95	2.61	12.83	7.78	7.20
Ta	0.15	0.29	0.30	0.01	0.23	0.06	0.62	0.55	0.41	0.55	0.64	0.49	0.68	0.69
Pb	2.00	2.61	4.98	2.69	8.74	3.70	6.28	6.79	5.53	7.06	12.18	5.64	15.99	15.17
Th	0.62	1.40	1.78	1.12	2.21	2.07	5.14	4.79	2.34	4.72	6.42	9.02	8.40	8.71
U	0.24	0.49	0.64	0.40	0.84	0.68	1.62	1.46	0.93	1.62	2.21	3.15	2.76	2.64

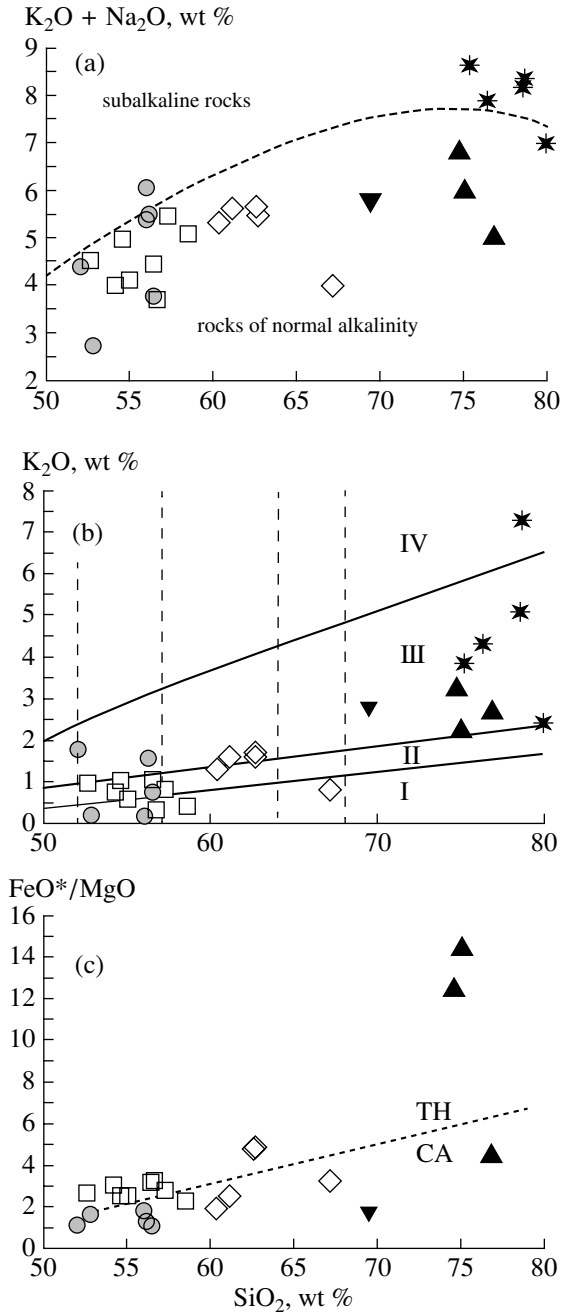

Fig. 6. Classification diagrams demonstrating the dualistic nature (affiliation with different series) of the Lower Paleocene hypabyssal rocks of the Omgon Range.
(a) $(Na_2O + K_2O) – SiO_2$ diagram (Wilson, 1989).
(b) $K_2O – SiO_2$ diagram (LeMaitre *et al.*, 1989).
(c) $FeO^*/MgO – SiO_2$ diagram (Miyashiro, 1974).
Magmatic series: I, TH—tholeiitic, II, CA—calc–alkaline, III—high-K calc–alkaline, IV—shoshonite. Other symbols are the same as in Fig. 5.

also typically enriched in LILE relative to HFSE and have negative anomalies at Nb (Nb/Nb* = 0.17–0.44) and Ta (Ta/Ta* = 0.08–0.29) (Figs. 9b, 9c), which suggest that the rocks could crystallize either from a melt derived from a source that had been recycled in a suprasubduction environment or from a melt contaminated with continental crustal rocks. In La/Yb–Th/Yb (Fig. 10a) and Nb/U–Nb (Fig. 10b) diagrams, the data points of the titanomagnetite gabbro-dolerites plot along the trends defined by the combined fractional crystallization of a melt derived from a depleted mantle source and the assimilation of continental crustal material by this melt.

The **biotite granites and granite-aplites** are meta- and peraluminous rocks of the calc–alkaline series (Fig. 6b). Their peraluminous varieties compose individual stratiform bodies, and the metaluminous rocks occur as relatively thin injections and dikes among ilmenite gabbro-dolerites.

The *peraluminous biotite granite and granite-aplite* have high aluminum saturation index [ASI = $Al_2O_3/(CaO + Na_2O + K_2O)_{mol}$ = 1.28–1.36] and high contents of normative corundum (3.01–5.88%), which are typical of S-granitoids, but exhibit some geochemical features similar to those of M- and I-granites (Chappel and White, 1974). The rocks are roughly equally enriched in K and Na (K_2O/Na_2O = 0.63–0.95) and have moderate K/Rb (256–289), Rb/Sr (0.48–0.81), and Rb/Ba (0.14–0.18) ratios. The biotite granite (sample O-27) is the least silicic of the granitoids and has the lowest initial $(^{87}Sr/^{86}Sr)_i$ ratio of 0.70387.

The peraluminous biotite granite and granite-aplites display moderately fractionated REE patterns with negative Eu anomalies (Eu/Eu* = 0.52–0.30). The $(La/Yb)_N$ ratio normalized to chondrite according to (Sun and McDonough, 1984) gradually decreases from 5.04 to 3.13–3.01 as the silicity of the rocks increases from 69.44 to 74.69–75.09 wt %. The concentrations of LREE and HREE in the granite-aplites are, respectively, ~2 and ~3.5 times higher than those in the least silicic biotite granite. The enrichment of the peraluminous granitoids in LILE relative to HFSE and the negative anomalies of the rocks at Nb (Nb/Nb* = 0.41–0.23), Ta (Ta/Ta* = 0.35–0.29), and Ti (0.35–0.09) (Fig. 9d) seem to have been inherited from the source of the melts. The concentration levels of Rb, Y, Nb, Yb, and Ta of the biotite granite correspond to those in granitoids in volcanic arcs, and those in the granite-aplites correspond to within-plate granitoids (Pearce, 1984).

Metaluminous granitoids [sample O-29(4)] have low ASI values (1.03) and are low in normative corundum (0.51%) but have several parameters close to those of the peraluminous granite-aplites described above. These rocks have identical patterns and concentrations of most lithophile elements (except only Zr and Hf), including REE [$(La/Yb)_N$ = 2.19, Eu/Eu* = 0.32], and have pronounced negative anomalies at Nb (Nb/Nb* = 0.22), Ta (Ta/Ta* = 0.37), and Ti (Ti/Ti* = 0.12) (Fig. 9d). The initial $(^{87}Sr/^{86}Sr)_i$ ratio of the metalumi-

nous granite-aplites varies from 0.70603 to 0.70680, which makes these rocks similar to postorogenic I granitoids and postcollisional (riftogenic) A granitoids.

PETROGENESIS OF HYPABYSSAL ROCKS IN THE OMGON RANGE

Genetic Relations between Hypabyssal Rocks of Different Associations

The associations of hypabyssal rocks distinguished in the Omgon Range were produced by the crystallization of melts of various compositions. The ilmenite and titanomagnetite gabbro-dolerites, which belong to the moderate- and high-Fe–Ti series, show different levels of their enrichment in lithophile elements at similar ranges of SiO_2 concentrations (Fig. 5), different rations of incompatible elements, such as Ta/Yb–Th/Yb (Fig. 8) and Th/Ta–La/Yb (Fig. 10a), and different initial Sr isotopic ratios (Table 9), which remain constant during the fractional crystallization of melts. The biotite granite, the least evolved rock among all of the granitoids (Table 7a), plots separately in binary diagrams and exhibits no direct relations with the mafic rocks (Fig. 5).

The rocks of the three series have different initial Sr ratios $(^{87}Sr/^{86}Sr)_i$ (Table 9), whose variations cannot be explained by either the fractional crystallization of a single melt or the combined fractional crystallization of a melt and its assimilation with the host mudstone and sandstone of the Omgon Group. The $(^{87}Sr/^{86}Sr)_i$ ratio of the ilmenite gabbro-dolerites decreases from 0.70532 to 0.70387 as the SiO_2 concentration increases from 51.97 to 56.41 wt %. The mudstone and sandstone of the Omgon Group have much higher $(^{87}Sr/^{86}Sr)_i$ ratios (0.70664–0.70683). The quartz microdiorites contain 60.33 wt % SiO_2 and have $(^{87}Sr/^{86}Sr)_i = 0.70457$, and the analogous values of the biotite granite are 69.44 wt % and 0.70390.

Evolution of the Basaltic Melts

In spite of the different enrichment levels of most major and lithophile elements in the ilmenite gabbro-dolerites, on the one hand, and in the titanomagnetite gabbro-dolerites, and quartz microdiorites, on the other, the rocks of these associations exhibit similar tendencies in their compositional variations, as can be seen in the variation diagrams (Fig. 5), and have similar mineral assemblages. These facts suggest that the ilmenite and titanomagnetite gabbro-dolerites and quartz microdiorites were produced by similar processes within the crust and can be considered together.

Multilevel Crystallization of Basite Melts

The ilmenite and titanomagnetite gabbro-dolerites and quartz microdiorites show evidence of crystallization at different depths. The pressure of the near-liquidus crystallization of clinopyroxene (Table 2) was evaluated by the geobarometer (Nimis, 1995). The high-Mg augite (generation I) in the cores of zonal clinopyroxene crystals in the ilmenite gabbro-dolerites ($Mg\#_{Cpx}$ = 86.1–83.3 and 84.8–81.9) crystallized at pressures of (3–4) ± 2 kbar, and the augite (generation I) in the cores of zonal clinopyroxene crystals in the titanomagnetite gabbro-dolerites and quartz microdiorites was formed at (6–7) ± 2 kbar ($Mg\#_{Cpx}$ = 77.5–74.4) and (2–3) ± 2 kbar ($Mg\#_{Cpx}$ = 67.9–65.9), respectively. The micropoikilophitic and microphitic textures, typical of dolerite patches in the mafic rocks, and the fission-track dates, which indicate that the terrigenous rocks were exhumed from depths of no less than 4 km in the Maestrichtian (~70 Ma) (Bogdanov *et al.*, 2003; Soloviev *et al.*, 2005), suggest that the gabbro-dolerites and quartz microdiorites crystallized near the surface in sills.

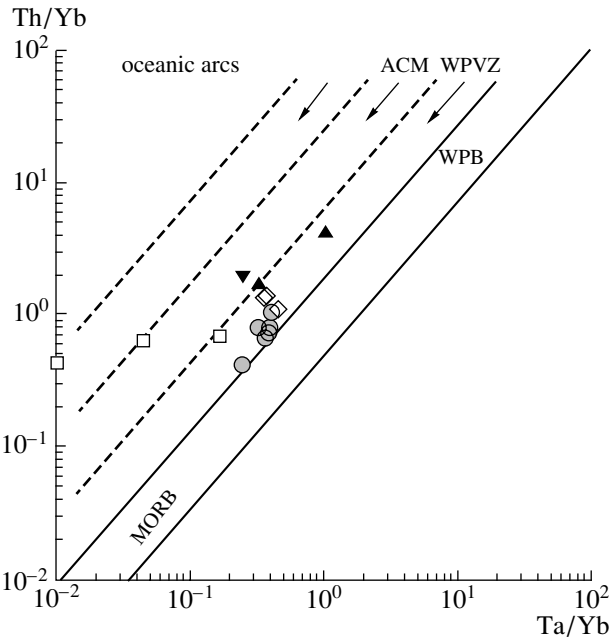

Fig. 7. Th/Yb–Ta/Yb diagram (Gorton and Schandl, 2000) demonstrating different ratios of highly incompatible elements in the hypabyssal rocks of the Omgon Range, the uncertain nature of the ilmenite gabbro-dolerites, and the similarity of the titanomagnetite gabbro-dolerites, quartz microdiorites, biotite granite, and granite-aplites to magmatic products at continental margins.

MORB—mid-oceanic ridge basalts, WPB—within-plate basalts, WPVZ—within-plate volcanic zones, ACM—active continental margins. See Fig. 5 for the explanations of other abbreviations.

Considered together with petrographic and geologic observations, the pressure evaluations made for the near-liquidus crystallization of clinopyroxene indicate that the mafic magmas crystallized in a series of deep-sitting magmatic reservoirs and, later, in sills near the surface.

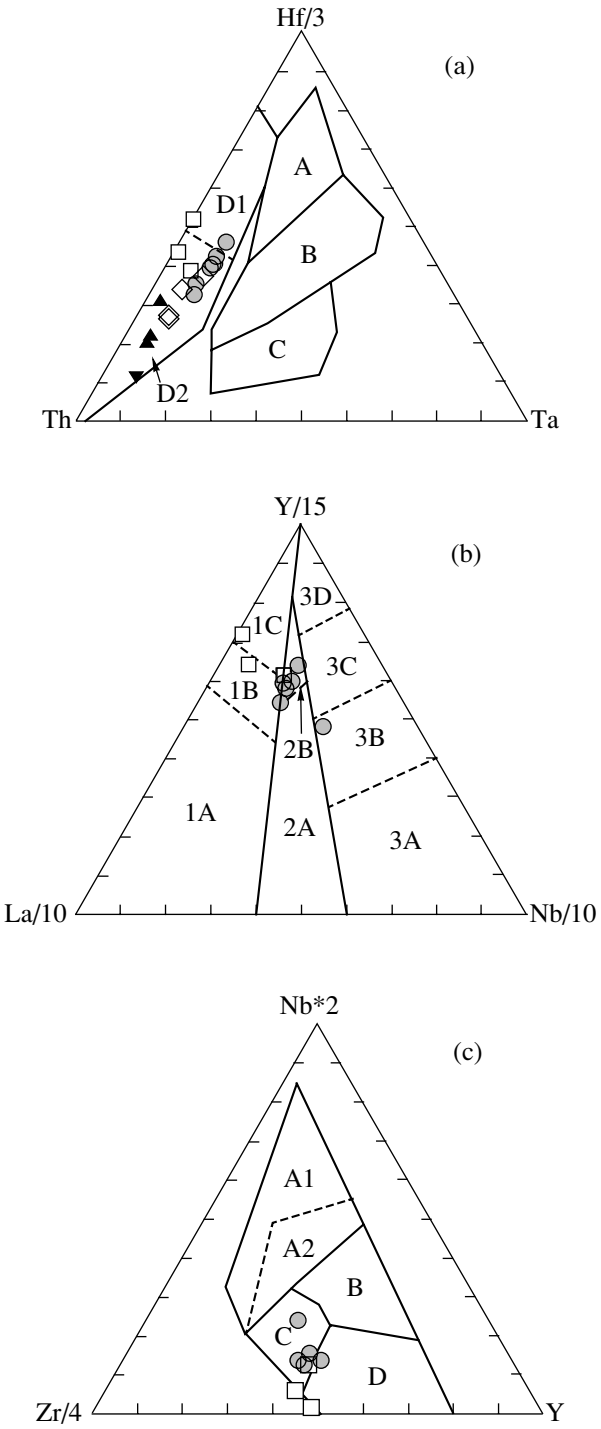

Evolution of Basite Melts in Deep-Sitting Chambers

Taking into account the textural and structural characteristics of the rocks and the evaluated pressures of the near-liquidus crystallization of their clinopyroxene (Table 2), it is reasonable to believe that the minerals of the deep associations of the ilmenite gabbro-dolerites and quartz microdiorites were, respectively, high-Mg augite and augite (generation I) that compose the cores of large zonal clinopyroxene crystals, plagioclase of bytownite-labradorite composition (generation I) that occurs as poikilitic inclusions in the high-Mg augite and augite, and phenocrysts of these minerals. The compositional variations of the clinopyroxene of generation I within a single sample (Fig. 4) can be explained by the fractional crystallization of the melt with the removal of calcic plagioclase and, perhaps, also ore minerals concentrating Cr_2O_3 [samples O-29, O-29(1), and O-29(2)] and TiO_2 (samples O-38 and O-40), which were not identified under a microprobe.

Evolution of Basite Melts in Sills

Contamination of basaltic magma and its crystallization products with acid melts. The temperatures and oxygen fugacity estimated by the ilmenite–titanomagnetite oxibarometer (Anderson and Lindsley, 1985) for the titanomagnetite gabbro-dolerites and quartz microdiorites indicate that their ore minerals crystallized under conditions close to the QFM buffer, at temperatures from ~820 ± 10°C to ~700 ± 10°C (Table 4). The constancy of the redox potential in the course of the temperature decrease was controlled by magma crystallization in a system open with respect to oxygen (Ghiorso and Carmichael, 1985). With regard for the Sr isotopic composition, this could be possible if the crystallizing basaltic magma was contaminated with a newly arriving magma portion or an acid melt. The possibility of basaltic magma buffering due to the assimilation of terrigenous rocks of the Omgon Group can be excluded due to the reasons discussed above.

Modeling. To test the hypothesis of the contamination of the mafic magmas with acid melts, we simulated the behavior of major and trace elements and Sr isotopes. The modeling for the *ilmenite gabbro-dolerites* was conducted for sample O-29(1), which has the most evolved composition (Table 7). The starting composition of the moderate-Fe–Ti basaltic magma was selected to be equal to that of the composition of sam-

Fig. 8. Tectonomagmatic diagrams demonstrating the dualistic geochemical characteristics of the Lower Paleocene hypabyssal rocks in the Omgon Range.

(a) Ta–Hf–Th discriminant diagram (Wood, 1980). Fields: A—N-MORB, B—E-MORB and within-plate tholeiites, C—within-plate alkaline basalts, D—volcanic-arc basalts, including D1—island-arc tholeiites, D2—calc–alkaline basalts.

(b) Nb–Y–La discriminant diagram (Cabanis and Lecolle, 1989). Fields: *1*—volcanic-arc basalts, including 1A—calc–alkaline basalts, 1B—calc–alkaline basalts and island-arc tholeiites, 1C—island-arc tholeiites, 2A—continental basalts, 2B—basalts of back-arc basins, 3A—alkaline basalts of continental rifts, 3B—enriched E-MORB, 3C—weakly enriched E-MORB, 3D—N-MORB.

(c) Y–Nb–Zr discriminant diagram (DePaolo and Wasserburg, 1989). Fields: A1—within-plate alkaline basalts, A2—within-plate alkaline basalts and within-plate tholeiites, B—E-MORB, C—within-plate tholeiites and oceanic-arc basalts, D—N-MORB and oceanic-arc basalts. Other abbreviations are as in Fig. 5.

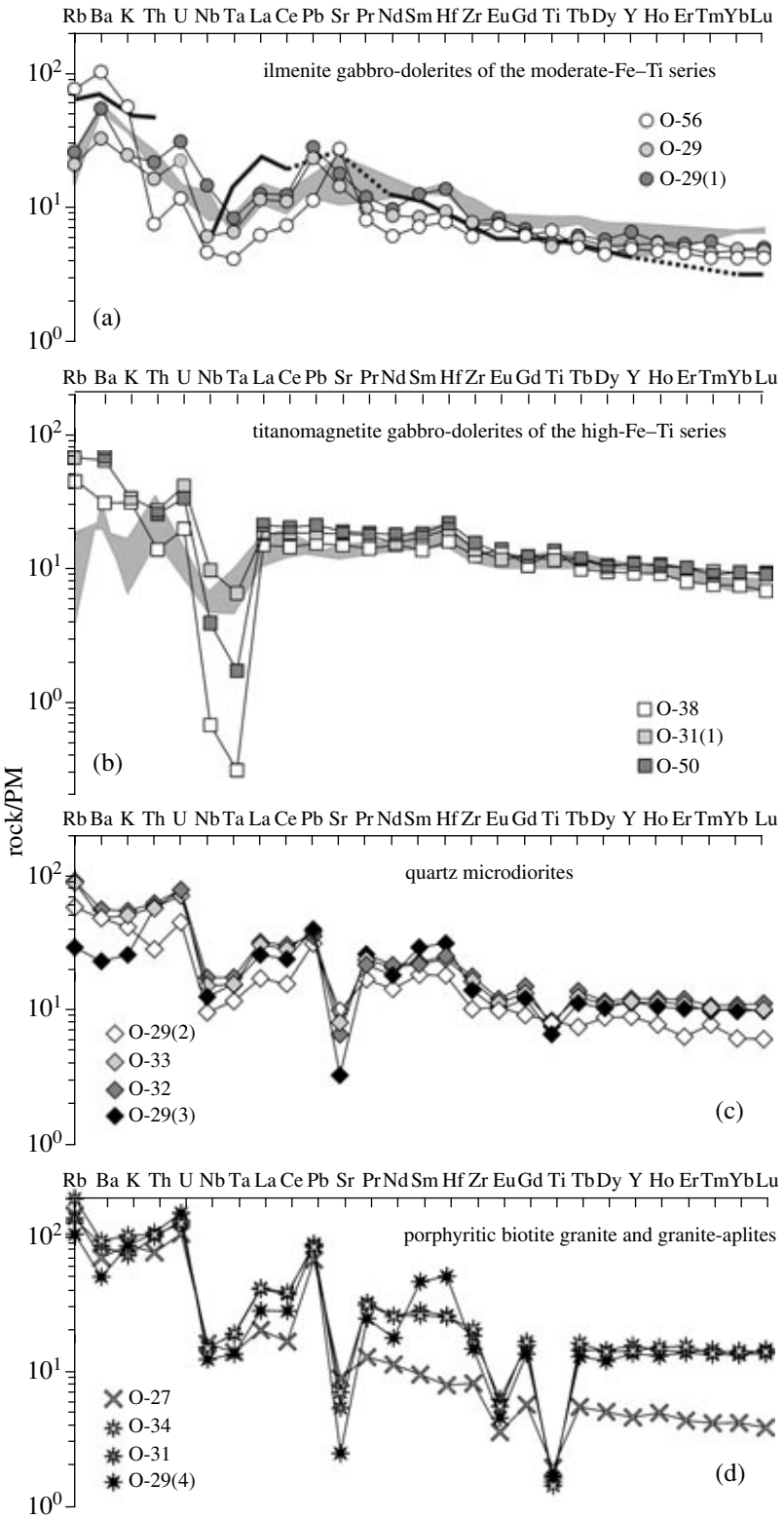

Fig. 9. Multielement patterns of the Lower Paleocene hypabyssal rocks of the Omgon Range. For comparison, the diagrams demonstrate similar patterns typical of the Upper Cretaceous–Middle Eocene volcanic rocks in extension zones in the continental margin of Northeast Asia (gray shading) (Fedorov and Filatova, 1999): (a) *Hy*-normative moderate-Ti tholeiitic basalts of Danian–Paleocene age from the Kakanaut area, (b) *Hy*-normative high-Ti tholeiitic basalts of Maestrichtian–Middle Eocene age from the Rarytkin area. The concentrations of elements are normalized to the primitive mantle (Hofmann, 1988).

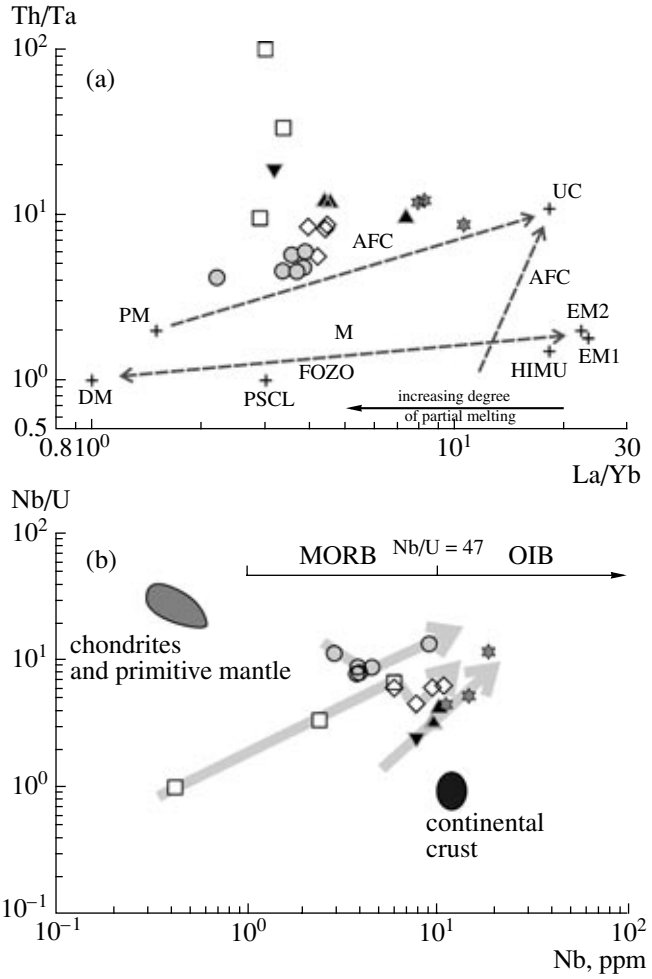

Fig. 10. Diagrams (a) La/Yb–Th/Ta (Condie, 1994) and (b) Nb–Nb/U (Hofmann, 1986) demonstrating the contributions of various sources to the genesis of the Omgon Range hypabyssal rocks.

Sources: DM—depleted mantle, PM—primitive mantle, PSCL—post-Archean subcontinental lithosphere, FOZO—universal mantle plume component, focus zone, EM1 and EM2—enriched mantle sources, HIMU—source enriched in radiogenic Pb because of a high μ value, UC—upper continental crust. Asterisks indicate the compositions of mudstones and sandstones of the Omgon Group. Processes: AFC—combined assimilation and fractional crystallization, M—mixing. MORB—mid-oceanic ridge basalts, OIB—oceanic-island basalts. Other symbols are the same as in Fig. 5.

ple O-56, which is characterized by negligibly low contribution of acid material, the lowest SiO_2 concentration among all of our samples, the lowest REE concentrations (Table 7), and the highest $(^{87}Sr/^{86}Sr)_i$ ratios (Table 9). The composition of the rhyolitic melt was assumed to correspond to that of sample O-27 of biotite granite, which is characterized by the lowest SiO_2 concentration among all of the granitoids (Table 7) and the lowest $(^{87}Sr/^{86}Sr)_i$ ratio (Table 9).

The behavior of major components and REE in the series of the ilmenite gabbro-dolerites can be best fitted by the model presuming a succession of (1) the mixing of the rhyolitic melt and a magma of moderate Fe–Ti basaltic composition and (2) the fractionation of the newly formed hybrid magma (Figs. 5, 11a). The major-component simulations with the use of the least-squares technique suggest the possible mixing of the basaltic magma and the rhyolitic melt in the proportion of 74.9 : 25.1.[2] However, the mixing of these components in the aforementioned proportion leads to much lower REE concentrations than those in the gabbro-dolerite of sample O-29(1) (Fig. 11a). The REE simulations of the fractional crystallization of the hybrid melt of the basaltic magma and rhyolitic melt yield values in good agreement with the natural rock at 27% fractionation of clinopyroxene, plagioclase, and ilmenite in the proportion 50 : 45 : 5 (Fig. 11a).[3] The behavior of Sr isotopes can be best described within the scope of the model of the combined fractional crystallization of a magma of moderate-Fe–Ti basaltic composition and the assimilation of a rhyolitic melt during the fractionation of 73% plagioclase and 23% orthoclase, with the degree of fractionation $F \le 0.68$ and the ratio of the assimilation rate to the crystallization rate $r = 0.7$.

The most realistic explanation of our simulation results seems to be the formation of the ilmenite gabbro-dolerites in the following stages: (i) the mixing of a moderate-Fe–Ti basite magma with a rhyolitic melt; (ii) the crystallization of the hybrid magma during the fractionation of clinopyroxene + plagioclase + ilmenite; and (iii) the crystallization of quartz + plagioclase + orthoclase from the acid melt. The results of these simulations make it possible to explain the succession of mineral assemblages crystallizing in the sills near the surface. Before the interaction of the basaltic magma and rhyolitic melt, the crystallizing assemblage had consisted of augite of generation II + hypersthene-bronzite + bytownite-labradorite of generation II + ilmenite + sphene. The emplacement of rhyolitic melt into the partly crystalline rocks induced a drastic

[2] The mixing of compositions O-56 and O-27 in this proportion yields $r^2 = 0.89$.

[3] The REE and Sr-isotopic simulation of the fractional crystallization was conducted by the algorithm (DePaolo, 1981). The partition coefficients of elements between minerals and melt ($KD^{mineral/melt}$) were compiled from (Rollinson, 1994). The modeling was carried out with the following values for the partition coefficients: $KD^{clinopyroxene/melt}$: *0.07* for La, 0.12 for Ce, *0.20* for Pr, 0.27 for Nd, 0.47 for Sm, 0.49 for Eu, 0.58 for Gd, 0.61 for Tb, 0.63 for Dy, 0.63 for Ho, 0.62 for Er, *0.60* for Tm, 0.58 for Yb, and 0.53 for Lu; $KD^{plagioclase/melt}$: *0.169* for La, 0.101 for Ce, *0.084* for Pr, 0.068 for Nd, 0.053 for Sm, 0.733 for Eu, 0.047 for Gd, *0.043* for Tb, 0.039 for Dy, *0.040* for Ho, 0.042 for Er, *0.043* for Tm, 0.045 for Yb, and 0.039 for Lu; $KD^{ilmenite/melt}$: 0.072 for La, 0.11 for Ce, 0.13 for Pr, 0.14 for Nd, 0.15 for Sm, 0.1 for Eu, 0.1 for Gd, 0.14 for Tb, *0.135* for Dy, 0.13 for Ho, *0.15* for Er, *0.16* for Tm, 0.17 for Yb, and *0.18* for Lu; $KD^{plagioclase/melt}$ for Sr is 6; $KD^{orthoclase/melt}$ for Sr is 9.4; values printed in italics are estimates.

change in the mineral assemblages and the onset of crystallization of high-Ca clinopyroxene of generation III + andesine–oligoclase of generation III + biotite + ilmenite + sphene and, later, quartz + albite ± orthoclase.

The behavior of major components and REE in the *titanomagnetite gabbro-dolerites and quartz diorites* [except samples O-29(2) and O-29(3)] can be described by a simple model of the mixing of a basaltic magma of high-Fe–Ti composition, which corresponds to that of sample O-38 of titanomagnetite gabbro-dolerite, and an acid melt, corresponding to sample O-31 of granite-aplite (Figs. 11b, 11c). The simulations with the compositions of samples O-50 and O-32 gave ideally consistent major-components and REE results. The insignificant deviation of the simulated REE from that of sample O-31(1) can be explained by somewhat different proportions of the mixing mafic and acid melts or the modification of the hybrid magma composition during its fractional crystallization.

The behavior of major components and REE in quartz microdiorite samples O-29(2) and O-29(3) is not consistent with any of the mixing models discussed above. It is reasonable to hypothesize that these quartz microdiorites, which compose a single thick sill with the ilmenite gabbro-dolerites, were produced by the fractional crystallization of a hybrid magma, whose composition corresponded to, for example, that of sample O-29(1) and which was generated by the mixing of a moderate Fe–Ti basaltic magma (sample O-56) and an uncontaminated rhyolitic melt (sample O-27). The behavior of major components suggests the principal possibility of this process (Fig. 5). The REE concentrations in the rock are lower than those in the gabbro-dolerites, which cab be explained by 10% fractionation of 40% clinopyroxene, 50% magnetite, and 10% titanomagnetite. This is, however, in conflict with nature observations. The inconsistency of our simulation results with natural observations can be explained by the fractionation of some hybrid compositions that were not identified in the course of our research.

Conditions and direction of mafic magma crystallization in the sills before their contamination with acid melts. Principal information on the conditions and direction of mafic magma crystallization in sills before the contamination of the magma with acid melts can be derived from the analysis of the mineral assemblage consisting of augite II + hypersthene-bronzite + bytownite-labradorite II ($An_{72.9–57.2}$ and $An_{56.6–49.1}$) + ilmenite (or ilmenite/titanomagnetite) + sphene. The chemistry of the clinopyroxene indicates that the leading process during this stage was the fractional crystallization of moderate- and high-Fe–Ti basic melts. This follows from the clearly pronounced normal zoning of augite of generation II, which suggests that the mineral crystallized simultaneously with calcic plagioclase, ilmenite, and titanomagnetite.

The temperature of the near-liquidus crystallization of the highest temperature augite and bronzite of this assemblage, which were, or almost were, in equilibrium in the ilmenite gabbro-dolerites, was estimated at ~1040–1050°C by the geothermometer (Wells, 1977) and at ~1000–1010°C by the geothermometer (Wood and Banno, 1973) (Table 2).[4] The crystallization temperature of the least magnesian augite and hypersthene that appeared in the same assemblage and started to crystallize in the course of magma crystallization was evaluated at ~900°C (Wells, 1997) and ~880°C (Wood and Banno, 1973). These temperature estimates are in good agreement with the temperatures yielded by the geothermometer (Lindsley, 1983) and testify to a gradual decrease in the clinopyroxene crystallization temperature from ~950 to ~850°C (Fig. 3d).

The temperature estimates for pyroxene crystallization in the titanomagnetite gabbro-dolerites and quartz diorites are less reliable because of the absence of equilibrium (or quasiequilibrium) ortho- and clinopyroxene pairs. However, the use of the two-pyroxene geothermometer (Lindsley, 1983) is justified because the rocks contain widespread pseudomorphs of serpentine ± chlorite + magnetite after orthopyroxene. The pyroxenes crystallized at temperatures of 900–800°C (Fig. 3d).

Crystallization conditions and products of the basic magmas contaminated with acid melts. This evolutionary stage of the gabbro-dolerites and quartz diorites produced the assemblage of high-Ca clinopyroxene (generation III) + andesine-oligoclase (generation III) + biotite + ilmenite (or titanomagnetite) + sphene. The crystallization temperature of the high-Ca clinopyroxene (salite, ferrosalite, and high-Ca augite) in the outer rims of the crystals was evaluated using the geothermometer (Lindsley, 1983) and varied from 700 to 600°C (sample O-29) and from 600 to <500°C [sample O-29(1) and O-38] (Fig. 3d).

[4] The equilibrated or unequilibrated character of orho- and clinopyroxene was tested by the method proposed in (Nakamura and Kushiro, 1970; Hunter, 1998). For the equilibrium crystallization of ortho- and clinopyroxene, the Fe–Mg distribution coefficient between these minerals is calculated by the formula $KD^{Fe–Mg} = (X_{Mg}^{Opx}/(1 - X_{Mg}^{Opx}))*((1 - X_{Mg}^{Cpx})/X_{Mg}^{Cpx})$, where X_{Mg} = Mg/(Mg + Fe), mol, which should vary within the range of 0.75–1.08. Our calculations indicate that the high-Mg augite (generation I) that composes the cores of large grains has no equilibrium orthopyroxene counterpart. In the ilmenite gabbro-dolerites (sample O-29), bronzite (X_{Mg} = 0.71–0.73) could be in equilibrium (or almost in equilibrium) only with augite of elevated X_{Mg} (0.74). The KD^{Fe-Mg} is in this pair equal to 0.87–0.93. Hypersthene (X_{Mg} = 0.65) from the same sample could be in equilibrium (or in quasiequilibrium) with high-Ca ferroaugite and augite (X_{Mg} = 0.64–0.63) that compose the outermost rims of the crystals. Their KD^{Fe-Mg} varies within the range of 1.01–1.07. In the titanomagnetite gabbro-dolerites (sample O-38), we found no clinopyroxene in equilibrium (or in quasiequilibrium) with hypersthene (X_{Mg} = 0.51), possibly because of the small number of the analyzed grains.

Table 8. Concentrations (ppm) of trace elements in terrigenous rocks hosting sills in the Omgon Range

Component	OM-26[1]*	OM-36	O-28(4)
	mudstone		sandstone
Sc	20.81	19.07	12.50
Ti	5689.44	5574.43	6050.71
V	257.13	193.90	96.42
Cr	116.37	70.62	22.32
Mn	374.02	433.32	376.13
Co	24.36	13.82	13.26
Ni	59.86	35.26	22.73
Cu	35.53	33.87	17.29
Zn	134.10	115.00	58.21
Rb	66.11	103.41	68.53
Sr	287.45	135.64	107.93
Y	31.70	35.56	24.33
Zr	175.02	208.30	171.16
Nb	11.18	14.75	18.70
Cs	3.39	6.55	2.01
Ba	578.18	354.87	703.72
La	20.76	28.40	22.50
Ce	55.06	66.32	43.60
Pr	7.84	8.61	6.04
Nd	22.70	28.45	25.07
Sm	5.09	6.29	4.37
Eu	1.71	1.53	1.40
Gd	5.70	6.68	4.19
Tb	0.76	0.97	0.61
Dy	4.96	5.54	4.38
Ho	0.94	1.27	0.86
Er	2.79	3.83	2.15
Tm	0.51	0.55	0.39
Yb	2.54	3.62	2.15
Lu	0.44	0.59	0.33
Hf	5.61	5.29	4.67
Ta	0.58	0.83	0.71
Pb	13.55	19.10	10.77
Th	7.20	10.00	6.22
U	2.35	2.65	1.50

Evolution of the Acid Melt

Contamination of the Rhyolitic Melt with the Host Terrigenous Rocks of the Omgon Group

The initial $(^{87}Sr/^{86}Sr)_i$ ratio of the Biotite granite is equal to 0.70390 and increases to 0.70680 in the granite-aplites. This suggests that the granitoids were produced by the fractional crystallization of a rhyolitic melt and the simultaneous assimilation of crustal rocks. The most probable assimilants were mudstone and sandstone of the Omgon Group, whose xenoliths were found in the granite-aplites and whose $(^{87}Sr/^{86}Sr)_i$ ratios range from 0.70664 to 0.70683 (Table 9). To test this hypothesis, we simulated the behavior of REE and Sr isotopes (Fig. 11d). We assumed that the concentrations of REE and Sr isotopes in the parental melt correspond to those in the least evolved biotite granite of sample O-27, which has the lowest SiO_2 concentration among all of the granites and the lowest initial Sr isotopic ratio. The final derivative was assumed to be the granite-aplite of sample O-29(4) from a dike cutting across gabbro-dolerite. The rocks has the highest SiO_2 concentration and $(^{87}Sr/^{86}Sr)_i$ ratio. The results of our REE and Sr isotopic simulations are presented in Fig. 11d and are highly consistent with one another. The best agreement between the natural and simulated data takes place when 69% plagioclase, 10% orthoclase, 10% biotite, and 11% ilmenite fractionate from the acid melt at a degree of fractionation $F = 0.7$ and the ratio of the assimilation rate to the crystallization rate $r = 0.8$ (REE simulations) or 0.7 (simulations for Sr isotopes).

Melt Sources

Ilmenite and Titanomagnetite Gabbro-Dolerites

The genesis of the moderate- and high Fe–Ti basaltic melts is traditionally explained by different degrees of melting of a single source, different degrees of contamination of the parental melt with subcontinental lithospheric rocks (Condie, 2001 and references therein), and the heterogeneity of the mantle source. Our data indicate that the differences between the compositions of the ilmenite and titanomagnetite gabbro-dolerites, which are the crystallization products of, respectively, moderate- and high-Fe–Ti melts, cannot be explained by fractional crystallization, differences in the crystallization conditions, or the contamination of the same Basic melt with the host rocks of the Omgon Group or acid melts. The ilmenite and titanomagnetite gabbro-dolerites are the crystallization products of moderate- and high-Fe–Ti basaltic melts, which had been derived at different degrees of melting and at different depths, as follows from the differences between the Fe8 parameter (8.22 for the ilmenite gabbro-dolerites and 15.61 for the titanomagnetite gabbro-dolerites) and the (Ca/Al)8 ratio (0.58 and 2.30, respectively). These data indicate that the melts were derived from different mantle sources.

Both the high- and the moderate-Fe–Ti melts were derived from the depleted mantle: spinel peridotites that had been affected by melting and metasomatism before the Early Paleocene, in a region with subduction processes. The melting of spinel peridotites follows from the moderately fractionated character of the REE patterns, and the effect of subduction processes is evident from the enrichment of the gabbro-dolerites of both types in LILE relative to HFSE and from the fact

that the rocks are depleted in Nb and Ta (Figs. 9a, 9b). Before their melting, the depleted-mantle sources have been variably depleted in such elements as Nb, Ta, Ti, and Zr. The metasomatic fluids were derived from the subducted plate, as follows from, for example, the high Ba/La and $(^{87}Sr/^{86}Sr)_i$ ratios at moderate Sr/Y values. The higher values of the Th/Nb, Ba/Nb, and U/Nb ratios of the titanomagnetite gabbro-dolerites suggest that the source of the high-Fe–Ti basaltic melt was more strongly recycled by fluids from the subducted plate than the source of the moderate Fe–Ti melt. The spatial combination of the crystallization products of these melts seems to reflect the vertical heterogeneity of the mantle.

Granitoids

The REE concentrations and patterns of the peraluminous biotite granite and granite-aplite are comparable with those of granitoids generated by the partial melting of both metabasalts and metamorphosed terrigenous rocks within the crust. However, taking into account the geochemistry of the rocks and the low initial Sr isotopic ratio of the biotite granite that is not contaminated by the host rocks of the Omgon Group, it is reasonable to suggest that the source of the rhyolitic melt most probably consisted of metabasaltic rocks of suprasubduction provenance.

Model for the Genesis of Hypabyssal Rocks in the Omgon Range

A principal model for the genesis of the Lower Paleocene hypabyssal rocks of the Omgon Range and their coeval analogues in western Kamchatka (Fig. 9a) is presented in Fig. 12.

The parental moderate- and high-Fe–Ti basaltic melts were derived at different degrees of the adiabatic melting of material at different depths within the lithospheric mantle, which had been affected by melting and metasomatized by fluids from the subducted plate before the Early Paleocene. When ascending to the surface, the parental melts were contaminated with continental lithospheric rocks (most probably, within the crust), filled magmatic reservoirs at different depths, and continued to evolve in these reservoirs by means of fractional crystallization. The emplacement of basaltic melt into crustal chambers was associated with the anatectic melting of the wall rocks, most probably, metabasalts of suprasubduction provenance. Anatectic melting resulted in a rhyolitic melt.

Ascending to the surface, the basaltic magmas transformed in deep magma chambers and the rhyolitic melt formed sills in the Omgon Range. In these bodies, the basaltic magmas were modified by the processes of fractionation and mixing (see above) and gave rise to ilmenite and titanomagnetite gabbro-dolerites and to quartz microdiorites. At the same depth, the rhyolitic melt fractionated, assimilated the host rocks of the Omgon Group, and produced biotite granite and granite-aplites.

During the final stage, the basaltic magmas, their derivatives, hybrid magmas (generated by the mixing of the basaltic magmas and acid melts), and the acid melts were erupted at the surface, as follows from the presence of basalts, andesites, dacite, and rhyolites, and corresponding tuffs in the Utkholok Peninsula.

GEODYNAMIC INTERPRETATIONS

The ilmenite and titanomagnetite gabbro-dolerites and related quartz microdiorites, biotite granites, and granite-aplites in the Omgon Range provide evidence of an extensional environment. This follows from:

(1) the simultaneous emplacement of moderate- and high-Fe–Ti mantle basaltic melts, as is typical of within-plate environments (Condie, 2001 and references therein);

(2) the similarities of several parameters of the ilmenite and titanomagnetite gabbro-dolerites with those of within-plate volcanics from areas of continental and backarc rifting (Figs. 7a, 9a, 9b);

(3) the identity of several parameters of the granitoids with those of postcollisional (riftogenic) A-granites.

Our materials and results indicate that, in contrast to what was thought previously (Shantser and Fedorov, 1997), the Early Paleocene hypabyssal rocks of the Omgon Range do not belong to the Western Koryakia–Kamchatka (Kinkil') volcanic belt. These rocks were formed earlier than this volcanic belt, perhaps, in relation to extension in the Eurasian continental margin. This process also occurred elsewhere in the region in Maestrichtian time (see, for example, Filatova, 1988; Fedorov and Filatova, 1999). The Lower Paleocene rocks of western Kamchatka and their compositional analogues of Paleocene age in this area lie in the continuation of the strike of a Late Senonian–Paleocene dike belt (Palandzhyan, 2002) and the field of the Maestrichtian–Upper Eocene basaltic complex (Filatova, 1988, 2000; Fedorov and Filatova, 1999), which mark Late Senonian–Middle Eocene extension in the Penzhina–Anadyr–Koryak area (Filatova, 1988, 2000; Fedorov and Filatova, 1999; Palandzhyan, 2002) (Fig. 1). In the Penzhina–Anadyr–Koryak area, Late Senonian–Paleocene plutonic complexes comprise small intrusions and dikes of alkaline and subalkaline microgranites, microsyenites, trachydacites, dacites, rhyolites, basaltic andesites, essexites, monzonites, syenites, and quartz diorite porphyries, which compose a belt extending for approximately 800 km (Palandzhyan, 2002). The volcanic complexes of Maestrichtian–Eocene age consist of basaltoids ranging from tholeiitic and moderate-Ti subalkaline to high-Ti olivine alkaline, sometimes in association with dacites and rhyolites (Fedorov and Filatova, 1999; Filatova, 2000). Comparing the compositions of the Early Pale-

Table 9. Whole-rock Rb–Sr isotopic data on hypabyssal magmatic and terrigenous rocks hosting them in the Omgon Range

Sample	Rb, ppm	Sr, ppm	$^{87}Rb/^{86}Sr$	±2σ	$^{87}Sr/^{86}Sr$	±2σ	$(^{87}Sr/^{86}Sr)_0$	±2σ	Age (Ma)
O-56	42.1	458.5	0.2658	0.0027	0.70556	0.00007	0.70532	0.00007	63.0
O-29(1)	14.7	337.4	0.1264	0.0013	0.70398	0.00007	0.70387	0.00007	63.0
O-29(2)	35.4	194.7	0.5257	0.0053	0.70504	0.00007	0.70457	0.00007	63.0
O-27	93.7	198.0	1.3688	0.0137	0.70512	0.00007	0.70390	0.00007	62.5
O-28(4)	68.1	135.4	1.4555	0.0146	0.70733	0.00007	0.70603	0.00007	63.0
O-29(4)	59.4	43.7	3.9303	0.0393	0.71032	0.00007	0.70680	0.00008	63.0
OM-26	66.1	212.1	0.9016	0.0090	0.70792	0.00007	0.70664	0.00007	99.8
OM-36	108.2	131.0	2.3894	0.0239	0.70973	0.00007	0.70683	0.00008	85.3

Note: The dates of the terrigenous rocks were compiled from (Bogdanov *et al.*, 2003).

ocene hypabyssal rocks from the Omgon Range and the Late Senonian–Eocene rocks from the Penzhina–Anadyr–Koryak area, we found out that some of the rocks are analogous. For example, the ilmenite gabbro-dolerites of the Omgon Range compositionally resemble the moderate-Fe–Ti tholeiitic basalts of Danian–Paleocene age in the Kakanaut area, and the titanomagnetite gabbro-dolerites are close to the Maestrichtian–Middle Eocene high-Fe–Ti basalts in the Rarytkin area (Fedorov and Filatova, 1999) (Figs. 1, 9a, 9b).

The causes of extension in western Kamchatka in the Early Paleocene are still not fully understood. None of the models proposed so far to account for the geodynamic evolution of the area takes into account extension in the Penzhina–Anadyr–Koryak area and western Kamchatka in the Maestrichtian–Middle Eocene, and none of these models can explain it. With regard for geological observations, the extension of the western Kamchatka segment of the Eurasian continental margin in Early Paleocene time can, theoretically, be related to (i) the termination of subduction beneath the Okhotsk–Chukchi volcanic belt in Campanian time and the subsequent "breakup" of the slab with the development of a mantle window; or (ii) the "roll-back" of the subducted slab with a drastic change in the geodynamic regime (Hourigan, 2003).

The reasons of the extension process will be hopefully elucidated by further research. Currently available data on the composition of the Lower Paleocene magmatic rocks in western Kamchatka are better consistent with the latter scenario. Major- and trace-element indicators identified in the hypabyssal rocks of the Omgon Range suggest that the moderate- and high-Fe–Ti basaltic melts were generated by the decompression melting of the lithospheric mantle, which had been enriched in components mobile in the fluid phase and did not exhibit evidence of its interaction with the asthenospheric mantle. It is most logical to hypothesize that the sources of the moderate- and high-Fe–Ti basaltic melts were metasomatized by fluids derived from the descending slab during the subduction of oceanic Izanagi (Kula) plates beneath the Eurasian continental margin in Albian–Early Campanian time (Filatova, 1988), before the onset of decompression melting in the Early Paleocene.

The western Kamchatka and Penzhina–Anadyr–Koryak areas are not the only examples of fields of "calc–alkaline" basalt–andesite and basalt–andesite–

Fig. 11. Simulation results on the processes that controlled the genesis of the Omgon Range hypabyssal rocks.

(a) The behavior of major and trace elements in the ilmenite (moderate-Fe–Ti) gabbro-dolerites [sample O-29(1)] can be described by a model including (1) mixing of the crystallization products of the moderate-Fe–Ti basaltic magma, whose composition corresponds to that of the ilmenite gabbro-dolerite (sample O-56), and a rhyolitic melt, whose composition corresponds to that of the biotite granite (sample O-27), in the proportion 74.9 : 25.1 with the origin of a hybrid magma; (2) 27% fractionation of plagioclase, clinopyroxene, and ilmenite in the proportions 50 : 45 : 5 from the resultant magma; and (3) the subsequent fractionation of sodic plagioclase and orthoclase in the proportion 73 : 27.

(b) The behavior of major and trace elements in the titanomagnetite gabbro-dolerites [samples O-31(1) and O-50] can be described by a simple model of the mixing of the crystallization products of the high-Fe–Ti basaltic magma (sample O-38) and the rhyolitic melt (sample O-31) variably contaminated with terrigenous rocks of the Omgon Group.

(c) The behavior of major and trace elements in the quartz microdiorites (sample O-32) can be described by the mixing of the crystallization products of the high-Fe–Ti basaltic magma (sample O-38) and rhyolitic melt (sample O-31).

(d) The behavior of major and trace elements in the granite-aplites [sample O-29(4)] can be described by the combined fractional crystallization of rhyolitic melt whose composition corresponds to that of biotite granite (sample O-27) and the assimilation of the host mudstones of the Omgon Group (sample OM-36).

AFC—combined assimilation and fractional crystallization, FC—fractional crystallization; F—degree of fractionation; M—mixing; *r*—ratio of the crystallization rate to the assimilation rate.

Pl—plagioclase, *Cpx*—clinopyroxene, *Ort*—orthoclase, *Bt*—biotite, *Ilm*—ilmenite.

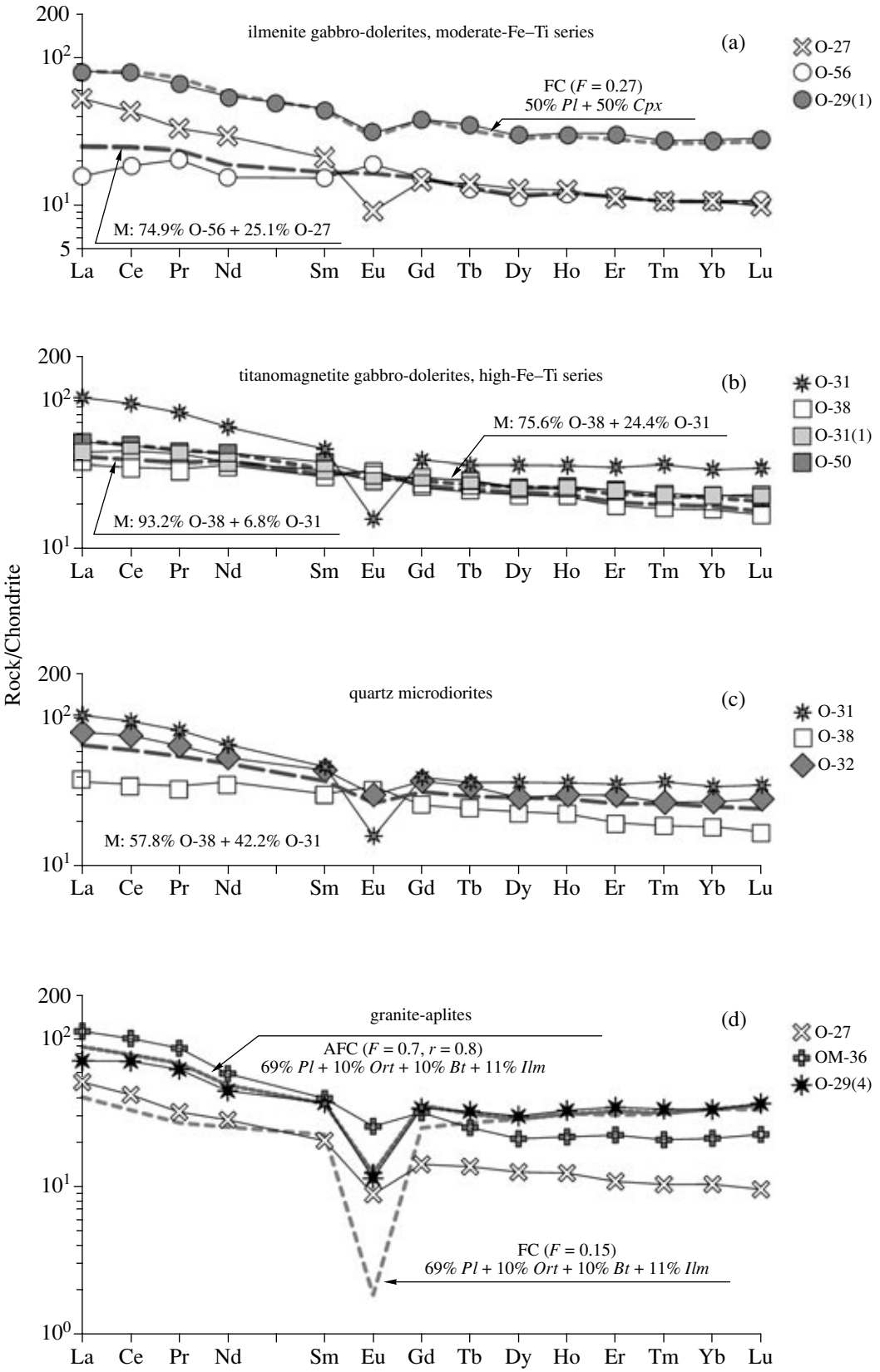
ilmenite gabbro-dolerites, moderate-Fe–Ti series
(a)
O-27
O-56
O-29(1)
FC (F = 0.27)
50% Pl + 50% Cpx
M: 74.9% O-56 + 25.1% O-27
titanomagnetite gabbro-dolerites, high-Fe–Ti series
(b)
O-31
O-38
O-31(1)
O-50
M: 75.6% O-38 + 24.4% O-31
M: 93.2% O-38 + 6.8% O-31
quartz microdiorites
(c)
O-31
O-38
O-32
M: 57.8% O-38 + 42.2% O-31
granite-aplites
(d)
O-27
OM-36
O-29(4)
AFC (F = 0.7, r = 0.8)
69% Pl + 10% Ort + 10% Bt + 11% Ilm
FC (F = 0.15)
69% Pl + 10% Ort + 10% Bt + 11% Ilm
Rock/Chondrite
200
10²
10¹
5
10⁰
La Ce Pr Nd Sm Eu Gd Tb Dy Ho Er Tm Yb Lu

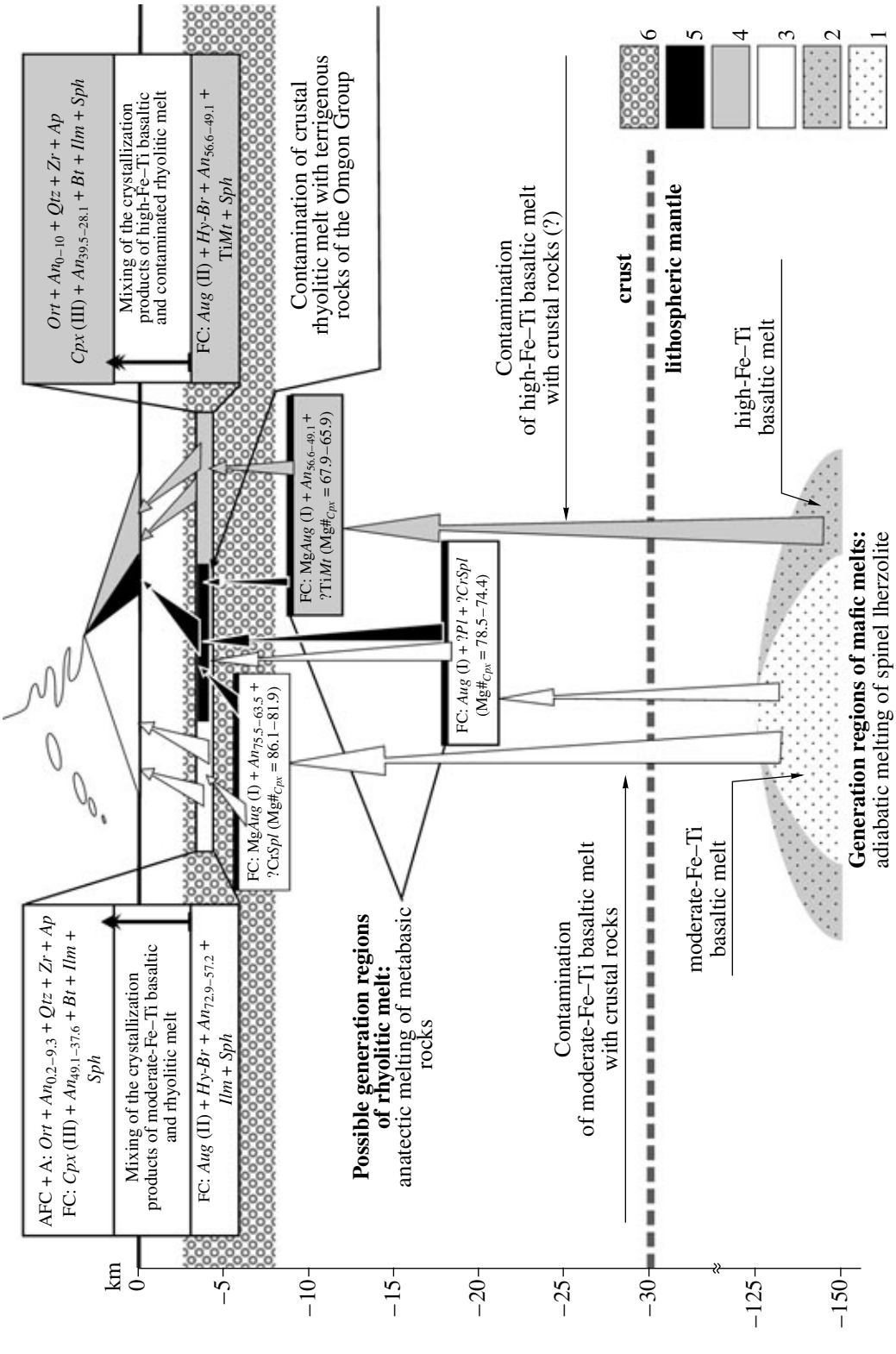

Fig. 12. Model for the genesis of the hypabyssal rocks of the Omgon Range during the extension of the subcontinental lithosphere of the ancient Eurasian continental margin. Magma-generation region: (1) moderate-Fe–Ti basaltic melt; (2) high-Fe–Ti basaltic melt. Crystallization products: (3) of moderate-Fe–Ti basaltic melt; (4) of high-Fe–Ti basaltic melt; (5) of rhyolitic melt; (6) area where terrigenous rocks of the Omgon Group occur.

Rectangles—crustal magmatic reservoirs, letters in them—processes that controlled the magma evolution and mineral assemblages. FC—fractional crystallization, AFC—combined fractional crystallization and assimilation, An_{0-100} plagioclase composition, *Ap*—apatite, *Aug*—augite, *Br*—bronzite, *Bt*—biotite, *Cpx*—clinopyroxene, Cr*Spl*—Cr-spinel, *Hy*—hypersthene, *Ilm*—ilmenite, Mg*Aug*—magnesian augite, *Ort*—orthoclase, *Pl*—plagioclase, *Qtz*—quartz, *Sph*—sphene, Ti*Mt*—titanomagnetite, *Zr*—zircon; (I), (II), (III)—associations I, II, and III; question marks mean that the occurrence of the mineral was inferred from the clinopyroxene composition.

dacite magmatism related to the extension of the continental lithosphere. Its classic examples include (i) the Basin and Range Province in the western North American coast (Robyn, 1979; Goles, 1986; Falkner *et al.*, 1995; Hawkesworth *et al.*, 1995; Hooper *et al.*, 1995, 2002; Johnson and Grunder, 2000; Morris *et al.*, 2000; Camp *et al.*, 2003), (ii) the coastal areas of central Queensland, West Australia (Ewart *et al.*, 1992), and (iii) the D'Entrecasteaux Islands, eastern Papua New Guinea (Smith, 1976; Smith and Milsom, 1984).

The uniqueness of the western Kamchatka segment of the Eurasian continental margin is underlain by the fact that this area, which suffered Early Paleocene extension, had a thick and probably hot continental lithosphere. The distance between preserved fragments of Paleocene volcanic centers in western Kamchatka reaches 350–400 km.[5] If the hypothesis that the volcanic centers developed above a magmatic diapir proves correct, then, taking into account the simplified scenario for the development of diapirs (Turcotte and Schubert, 1982), the thickness of the local lithosphere can be evaluated at 130–150 km. The significant thickness of the local lithosphere is also consistent with the 30-km thickness of the crust, the differentiated character of local magmatism, the occurrence of intermediate crustal chambers at different depths (21–18, 12–9, and 9–6 km), the generation of acid melts by means of anatectic melting, and the intensity of the assimilation of crustal rocks by the basaltic melts and the mixing of the crystallization products of the basaltic magmas and rhyolitic melts. This area can be ascribed to areas with hot continental lithosphere because it displays no evidence of brittle deformations (for instance, no dike fields) and the sporadic appearance of picrite–basaltic series (Khanchuk, 1985).

CONCLUSIONS

1. The hypabyssal rocks emplaced in the Upper Albian–Lower Campanian terrigenous deposits of the Eurasian collisional continental margin in the Omgon Range in western Kamchatka compose three coeval (62.5–63 Ma) rock associations: (i) ilmenite gabbro-dolerites, (ii) titanomagnetite gabbro-dolerites and quartz microdiorites, and (iii) porphyritic biotite granites and granite-aplites.

2. The ilmenite and titanomagnetite gabbro-dolerites were produced by the multilevel crystallization of moderate- and high-Fe–Ti basaltic melts that were contaminated with crustal material. The leading mechanism that controlled the compositional evolution of the magmas in the deep reservoirs was fractional crystallization. At shallow depths (3–4 km), the fractionation of the basaltic melts was complicated by their interaction with crustal rhyolitic melts.

3. The moderate- and high-Fe–Ti melts were derived from depleted mantle material: spinel peridotites, which were variably metasomatized and depleted by fluids derived from the slab that had been subducted before the onset of melting. The moderate- and high-Fe–Ti melts were generated at variable degrees of melting and at various depths, which seems to be indicative of the vertical compositional heterogeneity of the mantle.

4. The biotite granites and granite-aplites were produced by two combined processes: the fractional crystallization of a crustal rhyolitic melt and the assimilation of terrigenous rocks of the Omgon Group. The source of the rhyolitic melts seems to have consisted of suprasubduction rocks.

5. The genesis of the rock associations is related to extension in the margin of the Eurasian continent in Maestrichtian–Middle Eocene time (see, for example, Fedorov and Filatova, 1999). Early Paleocene extension in western Kamchatka and, as a consequence, the origin of the Lower Paleocene hypabyssal rocks of the Omgon Range and their volcanic analogues in Utkholok Peninsula and in the western slopes of the Sredinnyi Range of Kamchatka preceded the development of the Western Koryakia–Kamchatka volcanic belt.

ACKNOWLEDGMENTS

The authors sincerely thank the late N.A. Bogdanov for the financial support of the fieldwork in western Kamchatka in 1998. We appreciate cooperation with all members of the field team from the Institute of the Lithosphere of Marginal Seas, Russian Academy of Sciences. Invaluable help in the analytical work was provided by V.S. Bogatov (Institute of Mineralogy, Geochemistry, and Crystal Chemistry of Rare Elements), D.Z. Zhuravlev (same institute), and N.N. Karotaeva (Moscow State University). The authors also thank D.V. Kovalenko (Institute of the Geology of Ore Deposits, Petrography, Mineralogy, and Geochemistry, Russian Academy of Sciences), N.I. Filatova (Geological Institute, Russian Academy of Sciences), S.A. Palandzhyan (same institute), and the reviewers of this manuscript for the fruitful discussion of the materials and constructive criticism. This study was partly financially supported by the United States Civil-

[5] In the modern geologic structure of Kamchatka, exposures of Paleocene magmatic rocks are scarce and widely separated (Fig. 1). The Lower Paleocene rocks of Utkholok Peninsula and the hypabyssal rocks of the Omgon Range are scattered over an area of nearly 100 km across. The rock exposures occurring at a minimum distance from one another (a little bit more than 20 km) consist of the basalts and basaltic andesites of Utkholok Peninsula, which are compositionally close to the ilmenite gabbro-dolerites of the Omgon Range (Fig. 9a). This led us to suggest that the Lower Paleocene rocks of these two areas were formed within a single or several volcanic centers, above a single magmatic diapir. Moreover, volcanics of intermediate and acid composition (Cherepanov Series) dated at 59–65 Ma and their subvolcanic analogues dated at 55 Ma (Slyadnev *et al.*, 1997) were found in the foothills of the western surroundings of the Sredinny Range of Kamchatka, where they form an area extending for approximately 70 km at a maximum width of about 20 km.

ian Research and Development Foundation for the Independent States of the Former Soviet Union (Grant RG1-2568-MO-03), the Russian Foundation for Basic Research (project no. 04-05-64025), and a grant under the Program for Leading Research Schools of the Russian Federation (NSH-1980.2003.5).

REFERENCES

1. D. J. Anderson and D. H. Lindsley, "New (and Final!) Models for the Ti-Magnetite/Ilmenite Geothermometer and Oxygen Barometer," EOS Transis. **66**, 416 (1985).
2. N. A. Bogdanov and V. D. Chekhovich, "On the Collision between the West Kamchatka and Sea of Okhotsk Plates," Geotektonika, No. 1, 72–85 (2002) [Geotectonics **36** (1), 63–75 (2002)].
3. N. A. Bogdanov, "Tectonic Evolution of the Region," in *Explanatory Notes. Tectonic Map of the Sea of Okhotsk Region. Scale 1 : 2500000*, Ed. by N. A. Bogdanov and V. E. Khain (Inst. Litosf. Okrain. Vnutr. Morei, Ross. Akad. Nauk, Moscow, 2000), pp. 163–173 [142–151 (2000)].
4. N. A. Bogdanov, A. V. Solov'ev, G. V. Ledneva, *et al.*, "The Structure of the Cretaceous Accretionary Prism in the Omgon Range, West Kamchatka," Geotektonika, No. 4, 64–76 (2003) [Geotectonics **37**, 316–327 (2003)].
5. N. A. Bogdanov, G. E. Bondarenko, V. S. Vishnevskaya, and I. N. Izvekov, "Middle–Upper Jurassic and Lower Cretaceous Radiolarian Complexes of the Omgon Range, West Kamchatka," Dokl. Akad. Nauk SSSR **321** (2), 344–348 (1991).
6. G. E. Bondarenko and V. A. Sokolkov, "New Data on the Age, Structure, and Formation Conditions of the Omgon Volcanic–Siliceous–Carbonate Complex, West Kamchatka" Dokl. Akad. Nauk **315** (6), 1434–1437 (1990).
7. M. T. Brandon and J. A. Vance, "Tectonic Evolution of the Cenozoic Olympic Subduction Complex, Western Washington State, as Deduced from Fission–Track Ages for Detrital Zircon," Am. J. Sci. **292**, 565–636 (1992).
8. B. Cabanis and M. Lecolle, "Le Diagramme La/10–Y/15–Nb/8: Un Outil Pour la Discrimination des Series Volcaniques et la Mues en Evidence des Processus de Mélange et/ou de Contamination Crustale," C.R. Acad. Sci., Ser. II **309**, 2023–2029 (1989).
9. V. E. Camp, M. E. Ross, and W. E. Hanson, "Genesis of Flood Basalts and Basin and Range Volcanic Rocks from the Steens Mountain to the Malheur River Gorge, Oregon," GSA Bull. **115**, 101–128 (2003).
10. B. W. Chappel and A. J. R. White, "Two Contrasting Granite Types," Pacif. Geol. **8**, 173–174 (1974).
11. V. D. Chekhovich, N. A. Bogdanov, I. R. Kravchenko-Berezhnoi, *et al.*, *The Geology of West Bering Sea Area* (Nauka, Moscow, 1990) [in Russian].
12. E. E. Chernov and D. V. Kovalenko, "Paleomagnetism of Geological Complexes in the Omgon Range, West Kamchatka," Fiz. Zemli, No. 4, 1–10 (2001).
13. *Explanatory Notes to a Geological Map of the USSR 1:1000000, New Series, Page O-57: Palana* (VSEGEI, Leningrad, 1989) [in Russian].
14. K. C. Condie, "Greenstone Through Time," in *Archean Crustal Evolution*, Ed. by K. C. Condie (Elsevier, Amsterdam, 1994), pp. 85–120.
15. K. C. Condie, *Mantle Plumes and Their Record in Earth History* (Cambridge Univ. Press, Cambridge, 2001).
16. D. J. DePaolo and G. J. Wasserburg, "Inference about Magma Sources and Mantle Structure from Variations of $^{143}Nd/^{144}Nd$," Geophys. Rev. Lett. **3**, 743–746 (1976).
17. D. J. DePaolo, "Trace Elements and Isotopic Effects of Combined Wallrock Assimilation and Fractional Crystallization," Earth Planet. Sci. Lett. **53**, 189–202 (1981).
18. A. Ewart, R. W. Schon, and B. W. Chappell, "The Cretaceous Volcanic–Plutonic Province of the Central Queensland (Australia) Coast: A Rift Related 'Calc-Alkaline' Province," Trans. R. Soc. Edinburgh, Earth Sci. **83**, 327–345 (1992).
19. C. M. Falkner, C. F. Miller, J. L. Wooden, and M. T. Heizler, "Petrogenesis and Tectonic Significance of the Calc-Alkaline, Bimodal Aztec Wash Pluton, Eldorado Mountains, Colorado River Extension Corridor," J. Geophys. Res. **100**, 10453–10476 (1995).
20. P. I. Fedorov and N. I. Filatova, "Geochemistry and Petrology of Late Cretaceous and Cenozoic Basalts from Extensional Zones at the Continental Margin of Northeastern Asia," Geokhimiya, No. 2, 1–16 (1999) [Geochem. Int. **37** (2), 91–107 (1999)].
21. N. I. Filatova, *Perioceanic Volcanic Belts* (Nedra, Moscow, 1988) [in Russian].
22. N. I. Filatova, "Extension Zones of Continental Margins," in *Explanatory Notes. Tectonic Map of the Sea of Okhotsk Region. Scale 1 : 2500000*, Ed. by N. A. Bogdanov and V. E. Khain (Inst. Litosf. Okrain. Vnutr. Morei, Ross. Akad. Nauk, Moscow, 2000), pp. 46–48 [40 (2000)].
23. M. S. Ghiorso and I. S. E. Carmichael, "Chemical Mass Transfer in Magmatic Processes: II. Applications in Equilibrium Crystallization, Fractionation, and Assimilation," Contrib. Mineral. Petrol. **90**, 121–141 (1985).
24. Yu. B. Gladenkov, A. E. Shantser, A. I. Chelebaeva, V. N. Sinel'nikova, M. P. Antipov, V. N. Ben'yamovskii, M. G. Brattseva, B. P. Polyanskii, S. I. Stupin, and P. I. Fedorov, *The Lower Paleogene of Kamchatka* (GEOS, Moscow, 1997) [in Russian].
25. A. E. Goldyrev, "New Data on the Composition of Upper Cretaceous and Eocene–Oligocene Terrigenous Sequences in West Kamchatka, the Area of Moroshechnaya Mountain Range," in *Problems of Modern Geotectonics*, Ed. by N. A. Bogdanov, V. M. Moralev, and V. E. Verzhbitskii (Nauchnyi Mir, Moscow, 2001), pp. 136–138 [in Russian].
26. G. G. Goles, "Miocene Basalts of the Blue Mountains Province in Oregon: I. Compositional Types and Their Geological Settings," J. Petrol. **27** (Part 2), 495–520 (1986).
27. M. P. Gorton and E. S. Schandl, "From Continents to Island Arcs: A Geochemical Index of Tectonic Setting for Arc-Related and Within-Plate Felsic to Intermediate Volcanic Rocks," Am. Mineral. **38**, 1065–1073 (2000).
28. C. Guivel, Y. Lagabrielle, J. Bourgois, *et al.*, "New Geochemical Constraints for the Origin of the Ridge-

Subduction-Related Plutonic and Volcanic Suites from the Chile Triple Junction (Taitao Peninsula and Site 862, LEG ODP 141 on the Taitao Ridge)," J. South Am. Earth Sci. **311**, 83–111 (1999).

29. C. Hawkesworth, S. Turner, K. Gallagher, *et al.*, "Calc-Alkaline Magmatism, Lithospheric Thinning, and Extension in the Basin and Range," J. Geophys. Res. **100**, 10271–10286 (1995).
30. A. W. Hofmann, "Chemical Differentiation of the Earth: The Relationship between Mantle, Continental Crust, and Oceanic Crust," Earth Planet. Sci. Lett. **90**, 297–314 (1988).
31. A. W. Hofmann, "Nb in Hawaiian Magmas: Constraints on Source Composition and Evolution," Chem. Geol. **57**, 17–30 (1986).
32. P. R. Hooper, D. G. Bailey, and G. A. McCarley Holder, "Tertiary Calc-Alkaline Magmatism Associated with Lithospheric Extension in the Pacific Northwest," J. Geophys. Res. **100**, 10303–10319 (1995).
33. P. R. Hooper, G. B. Binger, and K. R. Lees, "Age of the Steens and Columbia River Flood Basalts and Their Relationship to Extension-Related Calc-Alkaline Volcanism in Eastern Oregon," GSA Bull. **114**, 43–50 (2002).
34. J. H. Hourigan, PhD Thesis (Stanford Univ., 2003).
35. A. G. Hunter, "Intracrustal Controls on the Coexisting Tholeiitic and Calc-Alkaline Magma Series at Aso Volcano, SW Japan," J. Petrol. **39**, 1255–1284 (1998).
36. A. J. Hurford, "Zeta: The Ultimate Solution to Fission–Track Analysis Calibration or Just an Interim Measure?," in *Advances in Fission–Track Geochronology* (Kluwer Academic, Boston, 1998), 19–32.
37. J. A. Johnson and A. L. Grunder, "The Making of Intermediate Composition Magma in a Bimodal Suite: Duck Butte Eruptive Center, Oregon, USA," J. Volcanol. Geotherm. Res. **95**, 175–195 (2000).
38. V. E. Khain and M. G. Lomize, *Geotectonics on a Geodynamic Basis* (Mosk. Gos. Univ., Moscow, 1995) [in Russian].
39. A. I. Khanchuk, *The Evolution of Ancient Sialic Crust of Island Arc Systems of Eastern Asia* (Dal'nevost. Nauchn. Tsentr, Akad. Nauk SSSR, Vladivostok, 1985) [in Russian].
40. E. A. Konstantinovskaya, "Geodynamics of Island Arc–Continent Collision in the Western Pacific Margin," Geotektonika, No. 5, 15–34 (1999) [Geotectonics **33** (5), 353–370 (1999)].
41. E. A. Konstantinovskaya, "Arc–Continent Collision and Subduction Reversal in the Cenozoic Evolution of the Northwest Pacific: An Example from Kamchatka (NE Russia)," in *Active Subduction and Collision in Southeast Asia (SEASIA)*, Ed. by S. Lallemand, C.-S. Liu, J. Angelier, and Y. B. Tsai (Elsevier, Amsterdam, 2001), pp. 75–94.
42. E. A. Konstantinovskaya, *Tectonics of East Asian Margins: Structural Development and Geodynamic Modeling* (Nauchnyi Mir, Moscow, 2003) [in Russian].
43. D. V. Kovalenko, *Paleomagnetism of Geological Complexes in Kamchatka and Southern Koryak Area: Tectonic and Geophysical Interpretations* (Nauchnyi Mir, Moscow, 2003) [in Russian].
44. D. V. Kovalenko, G. V. Ledneva, V. S. Vishnevskaya, T. B. Bayanova, *et al.*, "Lithotectonic Complexes and Tectonic Evolution of the Palana Island Arc, Western Kamchatka," Geotektonika, No. 6, 68–90 [Geotectonics **39** (6), 480–499 (2005)].
45. D. V. Kurilov, "New Finds of Jurassic–Cretaceous Radiolarians in West Kamchatka," in *Studies of the Lithosphere*, Ed. by V. M. Moralev (Inst. Litosf. Okrain. Vnutr. Morei, Ross. Akad. Nauk, Moscow, 2000), pp. 40–42 [in Russian].
46. A. B. Kuz'michev and N. A. Sukhov, "Cretaceous Deposits in the Island Arc Zone of Ust'-Palana Neighborhoods, West Kamchatka: Lithologic Column and Geodynamic Speculations," in *Studies of the Lithosphere*, Ed. by V. M. Moralev (Inst. Litosf. Okrain. Vnutr. Morei, Ross. Akad. Nauk, Moscow, 2000), pp. 33–36 [in Russian].
47. G. M. Laslett, P. F. Green, I. R. Duddy, and A. J. W. Gleadow, "Thermal Annealing of Fission Track in Apatite," Chem. Geol. **65**, 1–13 (1987).
48. R. W. LeMaitre, P. Bateman, and A. Dudek, *A Classification of Igneous Rocks and Glossary of Terms* (Blackwell, Oxford, 1989).
49. G. V. Ledneva, "Petrology and Geochemistry of Upper Cretaceous Magmatic Complexes in Western Kamchatka," in *Geology, Geochemistry, and Geophysics at the Boundary between the 20th and 21st Centuries*, Vol. 2: *Petrology, Geochemistry, Mineralogy, Geology of Ore Deposits, and Geoecology* (Svyaz' print, Moscow, 2002), pp. 131–133 [in Russian].
50. D. H. Lindsley, "Pyroxene Thermometry," Am. Mineral. **68**, 477–493 (1983).
51. A. Miyashiro, "Volcanic Rock Series in Island Arcs and Active Continental Margins," Am. J. Sci. **274**, 321–343 (1974).
52. G. A. Morris, P. B. Larson, and P. R. Hooper, "'Subduction Style' Magmatism in Non-Subduction Setting: The Colvill Igneous Complex, NE Washington State, USA," J. Petrol. **41**, 43–67 (2000).
53. Y. Nakamura and I. Kushiro, "Equilibrium Relations of Hypersthene, Pigeonite, and Augite in Crystallizing Magmas: Microprobe Study of Pigeonite Andesite from Weiselberg, Germany," Am. Mineral. **55**, 1999–2015 (1970).
54. P. Nimis, "A Clinopyroxene Geobarometer for Basaltic Systems Based on Crystal–Structure Modeling," Contrib. Mineral. Petrol. **121**, 115–125 (1995).
55. M. D'Orazio, F. Innocenti, P. Manetti, *et al.*, "The Quaternary Calc-Alkaline Volcanism of the Patagonian Andes Close to the Chile Triple Junction: Geochemistry and Petrogenesis of Volcanic Rocks from the Cay and Maca Volcanoes (~45°S, Chile)," South Am. Earth Sci. **16**, 219–242 (2003).
56. S. A. Palandzhyan, "The Western Koryak Belt of Dike and Hypabyssal Rocks as an Indicator of Extension and Destruction of the Fore-Arc of the Okhotsk–Chukot Volcanic Belt in the Late Senonian–Paleocene," Dokl. Akad. Nauk **385** (6), 800–804 (2002) [Dokl. Earth Sci. **385A** (6), 651–655 (2002)].
57. T. N. Palechek, A. V. Solov'ev, and M. N. Shapiro, "Structure and Age of Mesozoic Sedimentary-Volcanogenic

Deposits of the Palana Section (Western Kamchatka)," Stratigr. Geol. Korrelyatsiya **11** (3), 74–91 (2003) [Stratigr. Geol. Correlation **11** (3), 261–277 (2003)].

58. T. N. Palechek, E. Yu. Baraboshkin, A. V. Solov'ev, *et al.*, "A New Data on Structure and Age of Mesozoic and Cenozoic Deposits of Khairuzova Cape," in *Western Kamchatka: Mesozoic Geological Evolution*, Ed. by Yu.B. Gladenkov and S.A. Palandzhyan (Nauchnyi Mir, Moscow, 2005), pp. 77–91 [in Russian].
59. L. M. Parfenov and B. A. Natal'in, "Mesozoic–Cenozoic Tectonic Evolution of Northeast Asia," Dokl. Akad. Nauk SSSR **235** (2), 89–91 (1977).
60. J. A. Pearce, N. B. W. Harris, and A. G. Tindle, "Trace Element Discrimination Diagrams for the Tectonic Interpretation of Granitic Rocks," J. Petrol. **25**, 956–983 (1984).
61. T. L. Robyn, "Miocene Volcanism in Eastern Oregon: An Example of Calc-Alkaline Volcanism Unrelated to Subduction," J. Volcanol. Geotherm. Res **5**, 149–161 (1979).
62. H. R. Rollinson, *Using Geochemical Data: Evaluation, Presentation, Interpretation* (Essex, London, 1994).
63. N. I. Seliverstov, *The Bottom Structure in near-Kamchatka Water Areas and the Geodynamics of the Junction Zone of the Kuril–Kamchatka and Aleutian Island Arcs* (Nauchnyi Mir, Moscow, 1998) [in Russian].
64. A. E. Shantser and P. I. Fedorov, "Early Paleogene Volcanism," in *The Lower Paleogene of West Kamchatka: Stratigraphy, Paleontology, and Geological Events*, Ed. by Yu. B. Gladenkov (GEOS, Moscow, 1997), pp. 117–128 [in Russian].
65. M. N. Shapiro, "The Late Cretaceous Achaivayam–Valaginsky Volcanic Arc, Kamchatka, and the Plate Kinematics of North Pacific Zone," Geotektonika, No. 1, 58–70 (1995).
66. M. N. Shapiro, A. V. Solov'ev, G. I. Garver, and M. T. Brandon, "Sources of Zircons from Cretaceous and Lower Paleogene Terrigenous Sequences of the Southern Koryak Upland and Western Kamchatka," Litol. Polezn. Iskop., No. 4, 374–389 (2001) [Lithol. Miner. Resour. **36** (4), 322–336 (2001)].
67. G. P. Singaevskii and D. A. Babushkin, *Geological Map of the USSR, West Kamchatka, Pages O-57-XX and XIX* (VSEGEI, Leningrad, 1965) [in Russian].
68. B. I. Slyadnev, V. A. Sokolkov, and B. A. Markovskii, "Baraba Conglomerates, Kamchatka: Structure, Composition, and the Problem of Origin," Tikhookean. Geol. **16** (1), 83–88 (1997).
69. I. E. M. Smith and J. S. Milsom, "Late Cenozoic Volcanism and Extension in Eastern Papua," in *Marginal Basin Geology*, Ed. by M. Kokelaar and K. Howells, Geol. Soc. Spec. Publ. **16**, 163–171 (1984).
70. I. E. M. Smith, "Peralkaline Rhyolites from the D'Entrecasteaux Islands, Papua New Guinea," in *Volcanism in Australia*, Ed. by R. W. Johnson (Elsevier, New York, 1976), pp. 275–286.
71. A. V. Solov'ev, "Tectonics of Western Kamchatka: Constraints from Fission-Track and Structural Data," in *Western Kamchatka: Mesozoic Geological Evolution*, Ed. by Yu. B. Gladenkov and S. A. Palandzhyan (Nauchnyi Mir, Moscow, 2005), 163–194 [in Russian].
72. A. V. Soloviev, J. I. Garver, and G. V. Ledneva, J. Asian Earth Sci. (in press).
73. A. N. Sukhov and A. B. Kuz'michev, "Upper Cretaceous Deposits of Western Kamchatka," in *Western Kamchatka: Mesozoic Geological Evolution*, Ed. by Yu. B. Gladenkov and S. A. Palandzhyan (Nauchnyi Mir, Moscow, 2005), 121–162 [in Russian].
74. S. S. Sun and W. F. McDonough, "Chemical and Isotopic Systematics of Oceanic Basalts: Implication for Mantle Composition and Processes," in *Magmatism in Oceanic Basins*, Ed. by A. D. Saunders and M. J. Norry, Geol. Soc. Spec. Publ. **42**, 313–345 (1989).
75. *Tectonic Map of the Sea of Okhotsk Region 1:2500000*, Ed. by N. A. Bogdanov and V. E. Khain (Kom. Geod. Kartogr. Ross. Feder., Moscow, 2000) [in Russian].
76. *Tectonic Map of Northeast Asia 1 : 5000000*, Ed. by S. M. Tilman and N. A. Bogdanov (Kom. Geod. Kartogr. Ross. Feder., Moscow, 1992) [in Russian].
77. D. Turcotte and G. Schubert, *Geodynamics Applications of Continuum Physics to Geological Problems* (Wiley, New York, 1982; Mir, Moscow, 1985).
78. V. S. Vishnevskaya, I. A. Basov, T. N. Palechek, and D. V. Kurilov, "Radiolarians and Biostratigraphy of the Jurassic–Cretaceous Deposits of Western Kamchatka by Radiolarians and Foraminiferas," in *Western Kamchatka: Mesozoic Geological Evolution*, Ed. by Yu. B. Gladenkov and S. A. Palandzhyan (Nauchnyi Mir, Moscow, 2005), pp. 6–54 [in Russian].
79. V. S. Vishnevskaya, N. A. Bogdanov, and G. E. Bondarenko, "Middle Jurassic–Early Cretaceous Boreal Radiolarians from the Okhotsk Sea Coast of Kamchatka," Tikhookean. Geol. **17** (3), 22–35 (1998).
80. G. A. Wagner and P. Van den Haute, *Fission–Track Dating* (Kluwer, Dordrecht, 1992).
81. P. R. A. Wells, "Pyroxene Thermometry in Simple and Complex Systems," Contrib. Mineral. Petrol. **62**, 127–139 (1977).
82. M. Wilson, *Igneous Petrogenesis* (Unwin Hyman, London, 1989).
83. B. J. Wood and S. Banno, "Garnet–Orthopyroxene and Orthopyroxene–Clinopyroxene Relationships in Simple and Complex Systems," Contrib. Mineral. Petrol. **42**, 109–124 (1973).
84. D. A. Wood, "The Application of a Th–Hf–Ta Diagram to Problems of Tectonomagmatic Classification and to Establishing the Nature of Crustal Contamination of Basaltic Lavas of the British Tertiary Volcanic Province," Earth Planet. Sci. Lett. **50**, 11–30 (1980).
85. V. P. Zinkevich, E. A. Konstantinovskaya, N. V. Tsukanov, A. V. Rikhter, V. S. Kamenetskii, R. Magakyan, A. V. Sobolev, S. F. Karpenko, S. A. Garanina, L. V. Danyushevskii, N. N. Kononkova, M. V. Portnyagin, G. M. Kolesov, and T. V. Romashova, *Accretionary Tectonics of Eastern Kamchatka* (Nauka, Moscow, 1993) [in Russian].
86. L. P. Zonenshain, M. I. Kuz'min, and L. M. Natapov, *Plate Tectonics of the USSR Territory* (Nauka, Moscow, 1990) [in Russian].